# Model-based parameter estimation for characterizing wave propagation in a homogeneous medium

**James S. Hall and Jennifer E. Michaels**

School of Electrical and Computer Engineering, Georgia Institute of Technology, Atlanta, Georgia 30332-0250

E-mail: jennifer.michaels@ece.gatech.edu

**Abstract.** A model-based algorithm is presented that uses minimal *a priori* information and assumptions to adaptively estimate parameters associated with propagating waves in a homogeneous medium. These parameters include transmitter and receiver transfer functions, propagation distances, dispersion, and propagation loss. The algorithm is described in a general framework that accommodates direct arrivals from two or more transmitter-receiver pairs and can be readily adapted to handle application-specific model assumptions. Experimental validation is performed with two sets of ultrasonic guided wave data that conform to two different sets of model assumptions, demonstrating the impact of these assumptions and the ability to successfully estimate model parameters in a dispersive medium.



PACS numbers: 02.30.Zz,41.20.Jb,43.60.Uv,43.60.Pt,46.40.Cd

## 1. Introduction

Wave propagation is fundamental to a wide range of fields and applications, and many modern systems employing electromagnetic, acoustic or elastic waves require accurate knowledge of the operating environment to function properly. The performance of any of these systems is understandably linked to the accuracy of assumed propagation models and associated parameters, such as propagation distances, transmitter and receiver transfer functions, dispersion, propagation loss, etc. Errors in these *a priori* assumptions, caused by any number of factors, can impose an upper limit on a system's performance. This paper presents a model-based parameter estimation technique for wave propagation problems in which multiple signals are available for analysis. The approach can be tailored to application-specific model assumptions, including cases with multiple transmitter and receiver transfer functions.

To demonstrate the capabilities and adaptability of the parameter estimation algorithm, experimental validation is performed with two sets of ultrasonic guided wave data that conform to two different sets of model assumptions. Guided waves highlight the capabilities of this algorithm because they are dispersive and the transmitter and receiver transfer functions are typically transducer specific. The ability to simultaneously estimate transmitter and receiver transfer functions, propagation distances, and dispersion curves using minimal *a priori* information has direct applicability to structural health monitoring applications that employ guided waves with *in situ* sensors.

Inverse problems of acoustic and elastic waves generally attempt to estimate information about either the excitation source or the propagation medium. For example, source estimation algorithms can provide information about sources of seismic activity [1], underwater sound [2], or acoustic emission from cracks [3, 4]. Alternatively, information about the propagation medium is extracted for applications such as seismic exploration [5] and structural damage characterization [6, 7]. In contrast, the algorithm presented here leverages inherent model constraints to simultaneously characterize both the source and the propagation medium. Although such an ability has been demonstrated for other problems [8, 9], simultaneous estimation of both source characteristics and medium properties has not been achieved for signals recorded in a homogeneous, dispersive medium aside from earlier work by the authors. In Hall and Michaels [10], an application-specific model-based parameter estimation technique is presented as a method for characterizing the source waveform and propagation environment using a set of received guided wave signals. Similar to the model-based method proposed in this paper, the previously reported technique is capable of estimating dispersion relations, propagation distances, propagation loss, and the composite transmitter-receiver transfer function using minimal *a priori* information. However, unlike the algorithm presented here, the method reported in [10] requires identical transmitters and receivers as well as the presence of two propagating modes, which limits general applicability.

A number of techniques have been developed to estimate some of the specific wave propagation parameters estimated in the presented algorithm under various assumptions and constraints. A thorough review of this prior work is provided in Hall and Michaels [10] in the context of ultrasonic guided waves, where much of this work was on the estimation of dispersion relations. For example, if the propagation distances are known, then time-frequency representations are capable of graphically illustrating the frequency-dependent group velocities for dispersive waves [11, 12, 13]. Similarly, if a propagating wave is sampled at known, regularly spaced, and sufficiently close spatial intervals, Alleyne and Cawley [14] demonstrated that a two-dimensional (2D) Fourier transform can provide a graphical representation of the dispersion relations. In both of these cases, the resulting graphical image requires some additional post-processing to obtain numerical estimates. A third technique, the phase spectral analysis method, was originally proposed in 1977 by Sachse and Pao [15]. This technique obtains numerical estimates of the dispersion relations based on phase differences of the measured signals, assuming that the propagation distances and transmitted signal are known.

This paper is organized in the following manner. Section 2 presents the model-based parameter estimation algorithm, which is described in six separate stages: (1) problem setup, (2) expected noise behavior, (3) distance vector estimation, (4) linear solution, (5) nonlinear search, and (6) algorithm summary. Finally, Section 4 concludes the paper with a brief summary.

## 2. Parameter Estimation

### *2.1. Problem Setup*

A propagating wave can be modeled in the frequency domain as:

$$S(\omega) = T(\omega) R(\omega) G(\omega), \tag{1}$$

where $S(\omega)$ is the received signal; $T(\omega)$ is the transmitter transfer function, which incorporates all transmitter-specific transfer functions; $R(\omega)$ represents a similar combination of all receiver-specific transfer functions; and finally, $G(\omega)$ represents a distance-dependent transfer function that incorporates both propagation loss and dispersion. $G(\omega)$ can be modeled as

$$G(\omega) = \left(\frac{d}{\delta}\right)^{-p(\omega)} \exp\left(-\mathrm{i}k(\omega) d\right), \tag{2}$$

where $d$ is the propagation distance, $p(\omega)$ is referred to as propagation loss, $k(\omega)$ is a frequency-dependent wavenumber, and i is equal to $\sqrt{-1}$. The form of (2) is motivated by the well-known far-field behavior for both spherical and cylindrical waves [16], where dispersion is accounted for by the complex exponential term, and the geometric spreading loss, represented as $(d/\delta)^{-p(\omega)}$, is permitted to vary with frequency to accommodate possible frequency-dependent behavior. The $\delta$ variable embedded in the geometric spreading loss term accounts for the fact that the inverse

**Table 1.** Summary of working variables used throughout this paper.

| Variable | Size | Description |
|---|---|---|
| $\mathbf{S}_{\mathrm{m}}$ | $[3s \times w]$ | Frequency-domain data derived from recorded signals |
| $\vec{d}_{\mathrm{m}}$ | $[s \times 1]$ | Measured distances |
| $\vec{\sigma}^2_{\mathrm{m}}$ | $[s \times 1]$ | Measured noise variance |
| $\mathbf{S}_{\Re}$, $\mathbf{S}_{\Im}$ | $[s \times w]$ | Log-magnitude and phase responses of measured signals |
| $\mathbf{T}_{\Re}$, $\mathbf{T}_{\Im}$ | $[t \times w]$ | Transmitter-specific log-magnitude and phase responses |
| $\mathbf{R}_{\Re}$, $\mathbf{R}_{\Im}$ | $[r \times w]$ | Reciever-specific log-magnitude and phase responses |
| $\vec{p}$ | $[w \times 1]$ | Propagation loss vector |
| $\vec{k}$ | $[w \times 1]$ | Wavenumber vector |
| $\vec{d}$ | $[s \times 1]$ | Propagation distance vector |
| $\vec{d}^{\Upsilon}$ | $[s \times 1]$ | Logarithm of scaled propagation distance vector |
| $\vec{b}$ | $[s \times 1]$ | All integer vector associated with phase measurement |
| $\vec{1}_x$, $\vec{0}_x$ | $[x \times 1]$ | All ones or all zeros vector |
| $\mathbf{T}_{\Delta}$, $\vec{\tau}$ | $[t \times w]$,$[t \times 1]$ | Frequency-dependent (independent) components of $\mathbf{T}_{\Im}$ |
| $\mathbf{R}_{\Delta}$, $\vec{\rho}$ | $[r \times w]$,$[r \times 1]$ | Frequency-dependent (independent) components of $\mathbf{R}_{\Im}$ |
| $\vec{k}_{\Delta}$, $\kappa$ | $[w \times 1]$,$[1 \times 1]$ | Frequency-dependent (independent) components of $\vec{k}$ |
| $\mathbf{M}_{\mathrm{T}}$, $\mathbf{M}_{\tau}$ | $[s \times t]$ | Relates measurements in $\mathbf{S}$ to $\mathbf{T}$ estimates |
| $\mathbf{M}_{\mathrm{R}}$, $\mathbf{M}_{\rho}$ | $[s \times r]$ | Relates measurements in $\mathbf{S}$ to $\mathbf{R}$ estimates |
| $\mathbf{M}_{\mathrm{TR}}$, $\mathbf{M}_{\tau\rho}$ | $[s \times (t+r)]$ | Composite matrices ($[\ \mathbf{M}_{\mathrm{T}} \quad \mathbf{M}_{\mathrm{R}}\ ]$ and $[\ \mathbf{M}_{\tau} \quad \mathbf{M}_{\rho}\ ]$) |
| $\mathbf{M}^{\shortparallel}_{M}$ | $[s \times m^{\shortparallel}_{M}]$ | [a]Orthonormal basis for column space of $\mathbf{M}_M$ |
| $\mathbf{M}^{\curlywedge}_{M}$ | $[s \times (s - m^{\shortparallel}_{M})]$ | [a]Orthonormal basis for left null space of $\mathbf{M}_M$ |
| $\mathbf{M}^{\neq}_{M}$ | $[(t+r) \times m^{\neq}_{M}]$ | [a]Orthonormal basis for null space of $\mathbf{M}_M$ |
| $\mathbf{P}^{\curlywedge}_{M}$ | $[s \times s]$ | [a]Projection matrix onto $\mathbf{M}^{\curlywedge}_{M}$ |
| $\mathbf{P}_{\Delta}$ | $[w \times w]$ | Projection matrix onto null space of $\vec{1}^{\mathrm{T}}_{w}$ |
| $\mathbf{B}$ | $[s \times 3(t+r+1)+s]$ | Matrix used to isolate $\vec{b}$ elements ($[\ \mathbf{0} \quad \mathbf{I}_s\ ]$) |

[a] $M$ subscript may be either $TR$ or $\tau\rho$.

distance law only defines proportional relationships (nominally $d^{-1/2}$ or $d^{-1}$, depending on the application). Note that attenuation from a lossy medium can be handled by incorporating an exponential decay term, such as $\exp(-a(\omega)d)$, into (2) either in lieu of or in addition to the geometric spreading loss term. Since experimental validation is performed with guided waves, in which geometric spreading loss dominates attenuation, the algorithm is presented with geometric spreading loss.

The overarching goal of model-based parameter estimation is to obtain data-driven estimates of $T(\omega)$, $R(\omega)$, $d$, $p(\omega)$, and $k(\omega)$ by leveraging the inherent constraints of the assumed model in (1) and (2). The general approach to address this nonlinear problem is to convert it to a linear problem through the logarithm function:

$$\ln(S(\omega)) = \ln(T(\omega)) + \ln(R(\omega)) - p(\omega)\ln\left(\frac{d}{\delta}\right) - \mathrm{i}k(\omega)d + \mathrm{i}2\pi b. \quad (3)$$

When taking the logarithm of a complex number, the imaginary part of the result is constrained to be bounded by $\pm\pi$. Therefore, an integer multiple of $2\pi$ must be included in the phase, which necessitates the $\mathrm{i}2\pi b$ term in (3) where $b$ is an integer. Note that the the real and imaginary parts of (3) can be separated into two independent equations:

$$\ln(|S(\omega)|) = \ln(|T(\omega)|) + \ln(|R(\omega)|) - p(\omega)\ln\left(\frac{d}{\delta}\right), \quad (4a)$$

$$\measuredangle S(\omega) = \measuredangle T(\omega) + \measuredangle R(\omega) - k(\omega)d + 2\pi b. \quad (4b)$$

From a practical standpoint, the received signals are assumed to be digitally sampled in the time domain and frequency-domain measurements are obtained via a fast Fourier transform (FFT). As such, the frequency-domain measurements correspond to measurements at discrete frequencies. If these discrete frequencies are spaced sufficiently close to one another, the received signal phase response can be unwrapped by adding or subtracting integer multiples of $2\pi$ to eliminate phase discontinuities. To ensure the phase unwrapping operation is performed accurately, the frequency domain measurements must span a continuous spectral band with positive SNR within each frequency bin. By unwrapping the spectrum, the $b$ in (4$b$) becomes consistent across the entire frequency spectrum, which provides an additional model constraint that can be leveraged during parameter estimation. A lower bound was developed previously [10] for the number of time-domain samples, $n$, required to produce sufficiently close sampling in $\omega$:

$$n > \frac{2\pi F_s d_{\max}}{v_{\min}\left[\pi - 2\sin^{-1}\left(\frac{1}{Q_{\min}}\right)\right]}, \quad (5)$$

where $F_s$ is the sampling frequency, $d_{\max}$ is the maximum distance propagated for any received signal, $v_{\min}$ is the minimum group velocity at any frequency, and $Q_{\min}$ is the minimum signal-to-noise ratio (SNR) for any frequency. Note that the number of time-domain samples, $n$, can be increased to satisfy (5) by padding the received signals with zeros and does not translate to any system operational requirements.

To estimate the large number of unknowns in this problem, multiple $S(\omega)$ measurements are necessary. Therefore, multiple signals are recorded over different

propagation distances. The equations described in $(4a)$ and $(4b)$ can be converted into matrix format to relate information from each of the received signals to each of the parameters of interest:

$$\mathbf{S}_{\mathfrak{R}} = \mathbf{M}_{\mathrm{T}}\mathbf{T}_{\mathfrak{R}} + \mathbf{M}_{\mathrm{R}}\mathbf{R}_{\mathfrak{R}} - \vec{d}^{\,\Upsilon}\vec{p}^{\,\mathrm{T}}, \tag{6a}$$

$$\mathbf{S}_{\mathfrak{I}} = \mathbf{M}_{\mathrm{T}}\mathbf{T}_{\mathfrak{I}} + \mathbf{M}_{\mathrm{R}}\mathbf{R}_{\mathfrak{I}} - \vec{d}\,\vec{k}^{\,\mathrm{T}} + 2\pi\vec{b}\,\vec{1}_w^{\,\mathrm{T}}. \tag{6b}$$

Here matrices are represented by boldface font, vectors by $\vec{\cdot}$, and superscript "T" denotes a matrix or vector transpose operation. The "$\mathfrak{R}$" and "$\mathfrak{I}$" matrix subscripts denote the real and imaginary components of the logarithm of the data. The $\mathbf{S}_{\mathfrak{R}}$ and $\mathbf{S}_{\mathfrak{I}}$ matrices are $[s \times w]$ matrices containing all measured information, where $s$ is the number of received signals and $w$ is the number of frequencies. The $\mathbf{T}_{\mathfrak{R}}$ and $\mathbf{R}_{\mathfrak{R}}$ matrices correspond to the $t$ unknown $\ln(|T(\omega)|)$ and $r$ unknown $\ln(|R(\omega)|)$ estimates and the $\mathbf{T}_{\mathfrak{I}}$ and $\mathbf{R}_{\mathfrak{I}}$ matrices similarly correspond to the $t$ and $r$ unknown $\measuredangle T(\omega)$ and $\measuredangle R(\omega)$ variables, respectively. The $\mathbf{M}_{\mathrm{T}}$ and $\mathbf{M}_{\mathrm{R}}$ matrices relate each row of the $\mathbf{S}_{\mathfrak{R}}$ and $\mathbf{S}_{\mathfrak{I}}$ matrices to the appropriate row of $\mathbf{T}_{\mathfrak{R}}$, $\mathbf{T}_{\mathfrak{I}}$, $\mathbf{R}_{\mathfrak{R}}$, and $\mathbf{R}_{\mathfrak{I}}$. The elements of the $\mathbf{M}_{\mathrm{T}}$ and $\mathbf{M}_{\mathrm{R}}$ matrices are assumed to be limited to the integers "1" and "0", which is the case for all envisioned scenarios. This construction allows the model to account for either common or multiple transmitter and receiver transfer functions. The $\vec{p}$ and $\vec{k}$ vectors are $[w \times 1]$ vectors that contain the propagation loss and wavenumber estimates, respectively. The $\vec{b}$ vector contains each of the $s$ integers associated with the unknown multiples of $2\pi$. The $\vec{1}_w$ vector corresponds to a $[w \times 1]$ vector of all-ones. Finally, the "$\Upsilon$" superscript discriminates between the $[s \times 1]$ vector, $\vec{d}$, which contains the propagation distances in vector format, and the $[s \times 1]$ vector, $\vec{d}^{\,\Upsilon}$, corresponding to the element-wise logarithm of the propagation distances scaled by $\delta$:

$$\vec{d}^{\,\Upsilon} = \ln\left(\frac{1}{\delta}\vec{d}\right). \tag{7}$$

It is important to note that $\delta$ is an integral part of the assumed propagation model and will, therefore, affect the resulting estimates of $\mathbf{T}_{\mathfrak{R}}$, $\mathbf{R}_{\mathfrak{R}}$, and $\vec{p}$. Throughout this paper, the $\delta$ variable is selected to be the mean measured distance. Although this choice of $\delta$ is somewhat arbitrary, it has been found to produce reasonable estimates for all three parameters. Table 1 summarizes matrix and vector variables used throughout this paper.

Let $\mathbf{P}_{\Delta}$ be a $[w \times w]$ projection matrix ($\mathbf{P}_{\Delta}\mathbf{P}_{\Delta} = \mathbf{P}_{\Delta}$) corresponding to the null space of the all-ones row-vector, meaning that $\vec{1}_w^{\,\mathrm{T}}\mathbf{P}_{\Delta} = \mathbf{0}$. Then the $\mathbf{T}_{\mathfrak{I}}$ and $\mathbf{R}_{\mathfrak{I}}$ matrices of $(6b)$ can each be described in further detail as the addition of two separate components, one that is frequency-dependent, $\mathbf{T}_{\Delta}$ and $\mathbf{R}_{\Delta}$, and another that is frequency-independent, $\vec{\tau}$ and $\vec{\rho}$:

$$\begin{aligned} \mathbf{T}_{\mathfrak{I}} &= \mathbf{T}_{\Delta} + \vec{\tau}\,\vec{1}_w^{\,\mathrm{T}} \\ \mathbf{R}_{\mathfrak{I}} &= \mathbf{R}_{\Delta} + \vec{\rho}\,\vec{1}_w^{\,\mathrm{T}} \end{aligned} \tag{8}$$

where $\mathbf{T}_{\Delta} = \mathbf{T}_{\mathfrak{I}}\mathbf{P}_{\Delta}$ and $\mathbf{R}_{\Delta} = \mathbf{R}_{\mathfrak{I}}\mathbf{P}_{\Delta}$. The wavenumber vector can be similarly decomposed into:

$$\vec{k} = \vec{k}_{\Delta} + \kappa\vec{1}_w \tag{9}$$

with $\vec{k}_{\Delta}^{\mathrm{T}} = \vec{k}^{\,\mathrm{T}}\mathbf{P}_{\Delta}$. Note that the decomposition of $\mathbf{T}_{\Im}$, $\mathbf{R}_{\Im}$, and $\vec{k}$ into frequency-dependent and frequency-independent components is performed here for mathematical convenience and does not necessarily correspond to any physical properties or behavior.

To maximize the flexibility of the proposed model, two additional matrices, $\mathbf{M}_{\tau}$ and $\mathbf{M}_{\rho}$, are introduced to relate the frequency-independent values in $\vec{\tau}$ and $\vec{\rho}$ to each measurement in the $\mathbf{S}_{\Re}$ and $\mathbf{S}_{\Im}$ matrices. Under most circumstances, $\mathbf{M}_{\tau} = \mathbf{M}_{\mathrm{T}}$ and $\mathbf{M}_{\rho} = \mathbf{M}_{\mathrm{R}}$. However, there may be certain scenarios where the transmitter and receiver transfer functions are assumed to be identical, with the exception of some constant phase offset. In those cases, the $\mathbf{M}_{\tau}$ and $\mathbf{M}_{\rho}$ matrices may differ from $\mathbf{M}_{\mathrm{T}}$ and $\mathbf{M}_{\mathrm{R}}$. Incorporating (8) and (9) with (6*b*) yields:

$$\mathbf{S}_{\Im} = \mathbf{M}_{\mathrm{T}}\mathbf{T}_{\Delta} + \mathbf{M}_{\tau}\,\vec{\tau}\,\vec{1}_{w}^{\mathrm{T}} + \mathbf{M}_{\mathrm{R}}\mathbf{R}_{\Delta} + \mathbf{M}_{\rho}\,\vec{\rho}\,\vec{1}_{w}^{\mathrm{T}} - \vec{d}\,\vec{k}_{\Delta}^{\mathrm{T}} - \kappa\vec{d}\,\vec{1}_{w}^{\mathrm{T}} + 2\pi\vec{b}\,\vec{1}_{w}^{\mathrm{T}}. \tag{10}$$

Since, by definition, $\mathbf{T}_{\Delta}$ and $\mathbf{R}_{\Delta}$ reside in the null space of the all-ones row-vector, another set of equations can be obtained from (10) by right-multiplying $\mathbf{S}_{\Im}$ with $\mathbf{P}_{\Delta}$:

$$\mathbf{S}_{\Im}\mathbf{P}_{\Delta} = \mathbf{M}_{\mathrm{T}}\mathbf{T}_{\Delta} + \mathbf{M}_{\mathrm{R}}\mathbf{R}_{\Delta} - \vec{d}\,\vec{k}_{\Delta}^{\mathrm{T}}. \tag{11}$$

The matrices in (6*a*), (10) and (11) can be consolidated into a single set of linear equations:

$$\mathbf{A}\mathbf{X} = \mathbf{S}_{\mathrm{m}}, \tag{12}$$

where

$$\mathbf{A} = \begin{array}{c} \begin{array}{cccccccccc} (\underline{1}) & (\underline{2}) & (\underline{3}) & (\underline{4}) & (\underline{5}) & (\underline{6}) & (\underline{7}) & (\underline{8}) & (\underline{9}) & (\underline{10}) \end{array} \\ \left[\begin{array}{cccccccccc} \mathbf{M}_{\mathrm{T}} & \mathbf{0} & \mathbf{0} & \mathbf{M}_{\mathrm{R}} & \mathbf{0} & \mathbf{0} & -\vec{d}^{\,\Upsilon} & \vec{0}_s & \vec{0}_s & \mathbf{0} \\ \mathbf{0} & \mathbf{M}_{\mathrm{T}} & \mathbf{M}_{\tau} & \mathbf{0} & \mathbf{M}_{\mathrm{R}} & \mathbf{M}_{\rho} & \vec{0}_s & -\vec{d} & -\vec{d} & 2\pi\mathbf{I}_s \\ \mathbf{0} & \mathbf{M}_{\mathrm{T}} & \mathbf{0} & \mathbf{0} & \mathbf{M}_{\mathrm{R}} & \mathbf{0} & \vec{0}_s & -\vec{d} & \vec{0}_s & \mathbf{0} \end{array}\right] \end{array}, \tag{13a}$$

$$\mathbf{X} = \begin{array}{c} \begin{array}{cc} (\underline{1}) & \\ (\underline{2}) & \\ (\underline{3}) & \\ (\underline{4}) & \\ (\underline{5}) & \\ (\underline{6}) & \\ (\underline{7}) & \\ (\underline{8}) & \\ (\underline{9}) & \\ (\underline{10}) & \end{array} \\ \left[\begin{array}{c} \mathbf{T}_{\Re} \\ \mathbf{T}_{\Delta} \\ \vec{\tau}\,\vec{1}_{w}^{\mathrm{T}} \\ \mathbf{R}_{\Re} \\ \mathbf{R}_{\Delta} \\ \vec{\rho}\,\vec{1}_{w}^{\mathrm{T}} \\ \vec{p}^{\,\mathrm{T}} \\ \vec{k}_{\Delta}^{\mathrm{T}} \\ \kappa\vec{1}_{w}^{\mathrm{T}} \\ \vec{b}\,\vec{1}_{w}^{\mathrm{T}} \end{array}\right] \end{array}, \qquad \text{and} \qquad \mathbf{S}_{\mathrm{m}} = \left[\begin{array}{c} \mathbf{S}_{\Re} \\ \mathbf{S}_{\Im} \\ \mathbf{S}_{\Im}\mathbf{P}_{\Delta} \end{array}\right]. \tag{13b}$$

Equation (12) represents the generalized propagation model in the format of a nonhomogeneous matrix equation. The matrix $\mathbf{S}_{\mathrm{m}}$ contains all frequency-domain measurements, $\mathbf{A}$ represents the assumed propagation model, and $\mathbf{X}$ consists of the unknown variables. Note that (13*a*) and (13*b*) represent a general structure for the matrices of (12) under the current model assumptions. Two specific examples for these

matrices are provided in section 3.2 and section 3.3. Alternative model assumptions can be accommodated by updating the $\mathbf{X}$ and $\mathbf{A}$ matrices accordingly. Also, it is important to point out that $\mathbf{A}$ does not contain all model constraints. Specifically, the elements of $\vec{b}$ are not constrained to be integers.

Throughout this paper, references are frequently made to the four vector subspaces defined by the fundamental theorem of linear algebra [17]: (1) the column space, range, or image, denoted by a "$\shortparallel$" superscript, (2) the left null space or cokernel, denoted by a "$\measuredangle$" superscript, (3) the null space or kernel, denoted by a "$\neq$" superscript, and (4) the row space or coimage, denoted by a "$=$". These four vector subspaces are used in reference to two matrices in particular, which have a profound impact on the algorithm's ability to estimate parameters:

$$\mathbf{M}_{\mathrm{TR}} = \left[ \begin{array}{cc} \mathbf{M}_{\mathrm{T}} & \mathbf{M}_{\mathrm{R}} \end{array} \right], \tag{14a}$$

$$\mathbf{M}_{\tau\rho} = \left[ \begin{array}{cc} \mathbf{M}_{\tau} & \mathbf{M}_{\rho} \end{array} \right]. \tag{14b}$$

Here both $\mathbf{M}_{\mathrm{TR}}$ and $\mathbf{M}_{\tau\rho}$ are $[s \times (t+r)]$ matrices. Applying this vector space notation, $\mathbf{M}^{\shortparallel}_{\mathrm{TR}}$ is a matrix of orthonormal column vectors that span the column space of $\mathbf{M}_{\mathrm{TR}}$. The size of $\mathbf{M}^{\shortparallel}_{\mathrm{TR}}$ is defined as $[s \times m^{\shortparallel}_{\mathrm{TR}}]$. Similar definitions can be made for the other three vector subspaces as well as for the $\mathbf{M}_{\tau\rho}$ matrix. Building upon the above notation, projection matrices onto these vector subspaces are denoted as $\mathbf{P}$ matrices with the appropriate superscripts and subscripts. So, $\mathbf{P}^{\measuredangle}_{\mathrm{TR}}$ is a $[s \times s]$ projection matrix that projects onto the vector subspace spanned by $\mathbf{M}^{\measuredangle}_{\mathrm{TR}}$ (i.e. $\mathbf{P}^{\measuredangle}_{\mathrm{TR}} = \mathbf{M}^{\measuredangle}_{\mathrm{TR}}(\mathbf{M}^{\measuredangle}_{\mathrm{TR}})^{\mathrm{T}}$). Note that since $(\mathbf{M}^{\measuredangle}_{\mathrm{TR}})^{\mathrm{T}}\mathbf{M}^{\shortparallel}_{\mathrm{TR}} = \mathbf{0}$, $\mathbf{P}^{\measuredangle}_{\mathrm{TR}}\mathbf{M}_{\mathrm{T}} = \mathbf{0}$ and $\mathbf{P}^{\measuredangle}_{\mathrm{TR}}\mathbf{M}_{\mathrm{R}} = \mathbf{0}$. Finally, note that the rank-nullity theorem relates the dimensionality of the column space, $m^{\shortparallel}_{\mathrm{TR}}$, and dimensionality of the null space, $m^{\neq}_{\mathrm{TR}}$:

$$m^{\shortparallel}_{\mathrm{TR}} + m^{\neq}_{\mathrm{TR}} = t + r. \tag{15}$$

One last observation about the structure of $\mathbf{A}$ is in regards to the rank of the matrix. The rank can be determined by examining linearly independent subsets of the columns of $\mathbf{A}$. Assuming that the number of unknown transmitter and receiver transfer functions is smaller than the number of received signals ($t+r < s$), then $\mathbf{M}_{\mathrm{TR}}$ and $\mathbf{M}_{\tau\rho}$ are not full rank. As such, $\vec{d}$ and $\vec{d}^{\,\Upsilon}$ are assumed to be linearly independent of $\mathbf{M}_{\mathrm{TR}}$ and $\mathbf{M}_{\tau\rho}$. Therefore, the columns (1), (4), and (7) from (13$a$) span a column space with $m^{\shortparallel}_{\mathrm{TR}} + 1$ dimensions. Similarly, the columns (2), (5), and (8) also span a column space of $m^{\shortparallel}_{\mathrm{TR}} + 1$ dimensions that is orthogonal to the span of columns (1), (4), and (7). Finally, the columns (3), (6), (9), and (10), which are linearly independent of the two previous groups, span an $s$-dimensional column space since column (10) contains an $[s \times s]$ identity matrix. Therefore, the rank of $\mathbf{A}$ is:

$$\mathrm{rank}\,(\mathbf{A}) = s + 2m^{\shortparallel}_{\mathrm{TR}} + 2. \tag{16}$$

### *2.2. Noise Analysis*

One issue when working with any parameter estimation algorithm is the impact of noise. If complex Gaussian white noise is assumed present in the measured frequency

spectrum, two separate noise distributions are present in the elements of $\mathbf{S}_{\mathfrak{I}}$ and $\mathbf{S}_{\mathfrak{R}}$, that of phase noise and log-magnitude noise, respectively. This section characterizes the noise distributions by determining their probability distribution functions (PDFs), mean, and variance.

Consider the case of a single noisy measurement, $S_{\mathrm{m}}$, that represents a single complex value, $S$, that has been corrupted with an additive, circularly symmetric (a.k.a. proper) complex Gaussian random variable, $N$, with zero mean and variance $\sigma_{\mathrm{N}}^2$:

$$S_{\mathrm{m}} = S + N. \tag{17}$$

The above equation can be described as a single, circularly symmetric complex Gaussian random variable with $\mu = S$. Recall that the PDF for a complex Gaussian random variable in a Cartesian coordinate system is:

$$p\left(x,y\right) = \frac{1}{2\pi\sigma_{\mathrm{x}}\sigma_{\mathrm{y}}}\exp\left(-\frac{1}{2}\left(\frac{\left(x-\mu_{\mathrm{x}}\right)^2}{\sigma_{\mathrm{x}}^2}+\frac{\left(y-\mu_{\mathrm{y}}\right)^2}{\sigma_{\mathrm{y}}^2}\right)\right). \tag{18}$$

Since the noise is circularly symmetric, $\sigma_{\mathrm{x}}^2 = \sigma_{\mathrm{y}}^2 = \frac{\sigma_{\mathrm{N}}^2}{2}$. Without any loss of generality, $S$ is taken to be $S = |S| + j0$, which means that $(\mu_{\mathrm{x}}, \mu_{\mathrm{y}}) = (|S|, 0)$. Substituting these values into (18) and converting to polar coordinates yields:

$$\begin{aligned} p_{S_{\mathrm{m}}}\left(r,\theta\right) &= p\left(r\cos\theta, r\sin\theta\right) \\ &= \frac{r}{\pi\sigma_{\mathrm{N}}^2}\exp\left(\frac{2r\left|S\right|}{\sigma_{\mathrm{N}}^2}\cos\theta - \frac{r^2+\left|S\right|^2}{\sigma_{\mathrm{N}}^2}\right), \end{aligned} \tag{19}$$

where $p_{S_{\mathrm{m}}}(r,\theta)$ is the PDF of $S_{\mathrm{m}}$ in terms of $r$ and $\theta$ assuming that $0 \leq \theta < 2\pi$ and $0 \leq r$. From (19), the log-magnitude and phase noise distributions can be characterized.

*2.2.1. Log-Magnitude Noise Distribution* Before the log-magnitude distribution can be obtained, the magnitude distribution must be characterized. The PDF of $|S_{\mathrm{m}}|$ in terms of $r$, $p_{|S_{\mathrm{m}}|}(r)$, can be found by integrating (19) over all $\theta$:

$$\begin{aligned} p_{|S_{\mathrm{m}}|}\left(r\right) &= \int_0^{2\pi} p_{S_{\mathrm{m}}}\left(r,\theta\right)d\theta \\ &= \frac{2r}{\sigma_n^2}\exp\left(-\frac{r^2+\left|S\right|^2}{\sigma_n^2}\right)I_0\left(\frac{2r\left|S\right|}{\sigma_n^2}\right), \end{aligned} \tag{20}$$

where $I_0\left(z\right)$ is a modified Bessel function of the first kind,

$$I_0\left(z\right) = \frac{1}{2\pi}\int_0^{2\pi}\exp\left(z\cos\theta\right)d\theta. \tag{21}$$

Equation (20) is then used to define the *additive* noise associated with $|S_{\mathrm{m}}|$,

$$|S_{\mathrm{m}}| = |S| + N_{|\cdot|}, \tag{22}$$

where $N_{|\cdot|}$ is a random variable with PDF derived from (20):

$$p_{|\cdot|}(\nu) = p_{|S_{\mathrm{m}}|}\left(\nu + |S|\right). \tag{23}$$

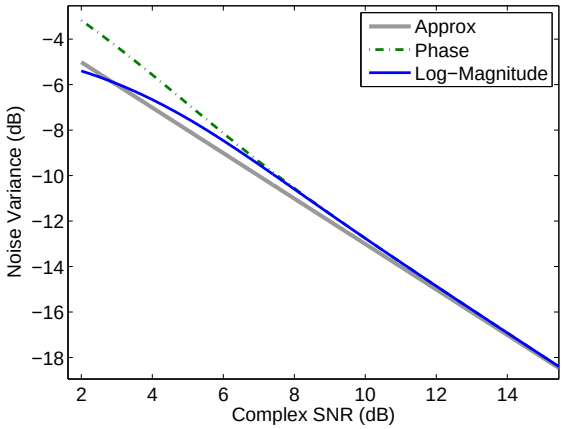


**Figure 1.** Log-magnitude and phase noise variance as a function of complex SNR. Note that the two analytic solutions closely match the approximation for SNR greater than 10 dB.

To find the PDF of the log-magnitude noise, note that:

$$\begin{aligned}\ln\left(|S_{\mathrm{m}}|\right) &= \ln\left(|S| + N_{|\cdot|}\right) \\ &= \ln\left(|S|\right) + \ln\left(1 + \frac{N_{|\cdot|}}{|S|}\right) \\ &= \ln\left(|S|\right) + N_{\ln|\cdot|}, \end{aligned} \tag{24}$$

where

$$N_{\ln|\cdot|} = \ln\left(1 + \frac{N_{|\cdot|}}{|S|}\right). \tag{25}$$

The above equation defines the log-magnitude noise, $N_{\ln|\cdot|}$, in terms of the magnitude noise, $N_{|\cdot|}$. Therefore, the PDF of the log-magnitude noise, $p_{\ln|\cdot|}(\nu)$, can be defined in terms of the magnitude PDF, $p_{|\cdot|}(\nu)$:

$$p_{\ln|\cdot|}(\nu) = p_{|\cdot|}(|S|\left(\exp\left(\nu\right) - 1\right)). \tag{26}$$

By combining (26), (23), and (20), the PDF of the log-magnitude noise distribution can be obtained:

$$\begin{aligned} p_{\ln|\cdot|}\left(\nu\right) &= p_{|S_{\mathrm{m}}|}\left(|S|\left(\exp\left(\nu\right) - 1\right) + |S|\right) \\ &= p_{|S_{\mathrm{m}}|}\left(|S|\exp\left(\nu\right)\right) \\ &= 2Q^2\exp\left(2\nu - Q^2\left(\exp\left(2\nu\right) + 1\right)\right) I_0\left(2Q^2\exp\left(\nu\right)\right), \end{aligned} \tag{27}$$

where $Q = |S|/\sigma_{\mathrm{N}}$ is referred to as the complex SNR.

Equation (27) indicates that the log-magnitude noise distribution, and therefore the resulting mean and variance, is dependent on the complex SNR. Figure 1 shows the log-magnitude noise variance vs. complex SNR. The same data are presented in figure 2 in the form of the log-magnitude noise standard deviation, which is plotted alongside the log-magnitude mean for direct comparison. Note that although the log-magnitude noise distribution has a *non-zero* mean, the mean is very small relative to the standard

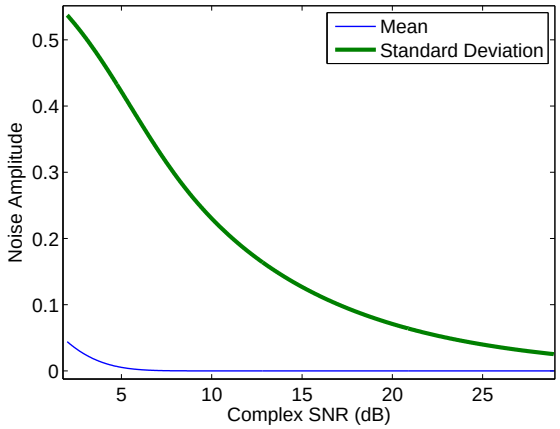


**Figure 2.** Mean and standard deviation of log-magnitude noise vs. complex SNR. Although log-magnitude noise has a non-zero mean, the mean is very small compared to the standard deviation.

deviation. As a result, it is reasonable to treat this distribution as having zero mean and there is little benefit to bias-compensation.

*2.2.2. Phase Noise Distribution* The probability distribution function of the phase noise, $p_{\measuredangle}(\theta)$, can be found by integrating (19) over $0 \leq r < \infty$, yielding the following result:

$$\begin{aligned} p_{\measuredangle}(\theta) &= \int_0^{\infty} p_{S_{\mathrm{m}}}(r,\theta)\, dr \\ &= \frac{1}{2\pi} \exp\left(-Q^2\right) \left(1 + Q\cos(\theta)\sqrt{\pi}\exp\left(Q^2\cos^2(\theta)\right)\left(1+\operatorname{erf}\left(Q\cos(\theta)\right)\right)\right), \end{aligned} \tag{28}$$

where

$$\operatorname{erf}(x) = \frac{2}{\sqrt{\pi}} \int_0^x \exp\left(-t^2\right) dt. \tag{29}$$

Similar to the case for the log-magnitude noise distribution, the phase noise distribution is a function of the complex SNR. Unlike the log-magnitude noise distribution, however, the phase noise distribution is zero mean. Figure 1 shows the phase-noise variance as a function of complex SNR. Note that as complex SNR increases, the phase and log-magnitude noise variances converge.

*2.2.3. Noise Variance Approximation* A linear approximation of the phase and log-magnitude noise variances as a function of complex SNR can be obtained by considering the case of a high SNR signal. Let $N_{\Re}$ and $N_{\Im}$ be the orthogonal components of the circularly symmetric complex noise variable, $N$, in the directions of the real and imaginary axes, respectively. As mentioned earlier, $N_{\Re}$ and $N_{\Im}$ each have zero mean and variance $\sigma^2_{\Re} = \sigma^2_{\Im} = \frac{\sigma^2_{\mathrm{N}}}{2}$. For a high SNR signal, the real and imaginary components of

the circularly symmetric noise effectively impact only magnitude and phase, respectively. As such, the phase noise variance is approximately:

$$\sigma_{\measuredangle}^2 \approx E\left[\arctan^2\left(\frac{N_{\Im}}{|S|}\right)\right] \approx \frac{1}{2Q^2}, \tag{30}$$

since $N_{\Im}/\,|S| << 1$ and the small angle approximation allows the arctan function to be approximated by its argument.

To obtain the log-magnitude approximation, note that log-magnitude noise is related to the magnitude noise in (25). As a result, the log-magnitude noise variance is effectively:

$$\sigma_{\ln|\cdot|}^2 \approx E\left[\ln^2\left(1+\frac{N_{\Re}}{|S|}\right)\right]. \tag{31}$$

For this high-SNR case, the logarithmic relationship can be simplified using the Taylor series expansion of a natural logarithm:

$$\begin{aligned}\ln\left(1+\frac{N_{\Re}}{|S|}\right) &= \frac{N_{\Re}}{|S|} - \frac{1}{2}\left(\frac{N_{\Re}}{|S|}\right)^2 + \frac{1}{3}\left(\frac{N_{\Re}}{|S|}\right)^3 - \cdots \\ &\approx \frac{N_{\Re}}{|S|},\end{aligned} \tag{32}$$

since $N_{\Re} << |S|$. Therefore, the log-magnitude noise variance can be approximated as $\sigma_{\ln|\cdot|}^2 \approx \frac{1}{2Q^2}$. This result is identical to the approximation for phase noise.

The phase and log-magnitude noise variance approximation is shown in figure 1 as a thick line for comparison with the analytic solutions. The analytic solutions clearly converge with the simple approximation and thus the approximation derived here can be considered valid for complex SNRs as low as 10 dB.

*2.2.4. Noise Model* The above analysis provides a mechanism to model the system noise in the logarithmic domain. Let the measurements contained in the measurement matrix, $\mathbf{S}_{\mathrm{m}}$, be modeled as a matrix of true values, $\mathbf{S}$, plus a matrix of additive noise, $\mathbf{N}$, similar to (17):

$$\mathbf{S}_{\mathrm{m}} = \mathbf{S} + \mathbf{N}. \tag{33}$$

The frequency-domain noise for each received signal is assumed to be circularly-symmetric i.i.d. Gaussian noise with variance $\sigma_{\mathrm{N}}^2$. Therefore, each column of $\mathbf{N}$ is independent of the other columns and has the structure:

$$\vec{N}_i = \left[\begin{array}{ccc} \vec{N}_{\Re i}^{\mathrm{T}} & \vec{N}_{\Im i}^{\mathrm{T}} & \vec{N}_{\Im i}^{\mathrm{T}} \end{array}\right]^{\mathrm{T}}, \tag{34}$$

where $\vec{N}_i$ is the $i^{\mathrm{th}}$ column of $\mathbf{N}$, and the $\vec{N}_{\Re i}$ and $\vec{N}_{\Im i}$ vectors correspond to the noise present in the $i^{\mathrm{th}}$ column of $\mathbf{S}_{\Re}$ and $\mathbf{S}_{\Im}$, respectively. Note that while the $\vec{N}_{\Re i}$ and $\vec{N}_{\Im i}$ vectors are independent of one another, the two $\vec{N}_{\Im i}$ vectors in the above equation, although not exactly the same as written, are *nearly identical* since the third set of linear equations corresponds to $\mathbf{S}_{\Im}\mathbf{P}_{\Delta}$, which effectively subtracts the row mean from each row and has a negligible impact on the noise. Since the phase noise and log-magnitude noise

can be treated as zero mean, the distribution for every element of $\mathbf{N}$ is assumed to have zero mean, $E[\mathbf{N}] = \mathbf{0}$. Further, by using the approximation from the previous section, $\sigma^2_{\ln|\cdot|} \approx \sigma^2_{\angle} \approx \frac{1}{2Q^2}$, the noise variance for each column can be approximated as:

$$\begin{aligned}\sigma_i^2 &= E\left[\vec{N}_i^{\mathrm{T}}\vec{N}_i\right] \\ &= E\left[\vec{N}_{\Re i}^{\mathrm{T}}\vec{N}_{\Re i}\right] + 2E\left[\vec{N}_{\Im i}^{\mathrm{T}}\vec{N}_{\Im i}\right] \\ &= \frac{3}{2}\sum_j \frac{1}{Q_{ij}^2},\end{aligned} \tag{35}$$

where $Q_{ij}$ is the complex SNR for the $i$th column (FFT frequency bin) and $j$th received signal.

### *2.3. Distance Vector Estimation*

To completely define $\mathbf{A}$ in (13$a$), the distance vector $\vec{d}$ must be known. Although it is possible to measure the propagation distances, these measurements are subject to measurement errors and may change slightly with variations in the propagation environment. As such, the measured distance vector, $\vec{d}_{\mathrm{m}}$, is constrained to fit the data.

To begin, the $s$-dimensional vector space that $\vec{d}$ resides in can be divided into two mutually exclusive subspaces based on the $\mathbf{M}_{\mathrm{TR}}$ matrix, $\mathbf{M}^{\shortparallel}_{\mathrm{TR}}$ and $\mathbf{M}^{\nparallel}_{\mathrm{TR}}$. Note that when the projection matrix, $\mathbf{P}^{\nparallel}_{\mathrm{TR}}$, is multiplied with the $\mathbf{S}_{\Im}\mathbf{P}_{\Delta}$ product described in (11), the distance vector term can be isolated:

$$\mathbf{P}^{\nparallel}_{\mathrm{TR}}\mathbf{S}_{\Im}\mathbf{P}_{\Delta} = -\mathbf{P}^{\nparallel}_{\mathrm{TR}}\vec{d}\,\vec{k}_{\Delta}^{\mathrm{T}}. \tag{36}$$

Inspection of the right-hand-side of (36) reveals that every column of $\mathbf{P}^{\nparallel}_{\mathrm{TR}}\mathbf{S}_{\Im}\mathbf{P}_{\Delta}$ is a scaled version of $\mathbf{P}^{\nparallel}_{\mathrm{TR}}\vec{d}$. Since $\vec{k}_{\Delta}^{\mathrm{T}}$ is unknown, $\vec{d}$ cannot be obtained directly. It is possible however, to use (36) to determine the *direction* of $\mathbf{P}^{\nparallel}_{\mathrm{TR}}\vec{d}$. Let $\vec{v}^{\nparallel}_{\mathrm{TR}}$ be the unit-norm vector corresponding to the direction of $\mathbf{P}^{\nparallel}_{\mathrm{TR}}\vec{d}$. Then $\vec{v}^{\nparallel}_{\mathrm{TR}}$ must satisfy:

$$\vec{v}^{\nparallel}_{\mathrm{TR}} = \arg\max_{\vec{v}} \vec{v}^{\mathrm{T}}\mathbf{V}\mathbf{V}^{\mathrm{T}}\vec{v}, \tag{37}$$

where $\mathbf{V}$ is defined as

$$\mathbf{V} = \mathbf{P}^{\nparallel}_{\mathrm{TR}}\mathbf{S}_{\Im}\mathbf{P}_{\Delta}. \tag{38}$$

Note that $\vec{v}^{\nparallel}_{\mathrm{TR}}$ is, by definition, the eigenvector that corresponds to the largest eigenvalue of $\mathbf{V}\mathbf{V}^{\mathrm{T}}$. Also, although not performed for the examples presented in this paper, more accurate estimates of $\vec{v}^{\nparallel}_{\mathrm{TR}}$ may be possible by normalizing or weighting the columns of $\mathbf{V}$ prior to performing the eigendecomposition.

The distance vector, $\vec{d}$, can now be defined in terms of $\vec{v}^{\nparallel}_{\mathrm{TR}}$, which is the unit-norm projection of $\vec{d}$ onto $\mathbf{M}^{\nparallel}_{\mathrm{TR}}$, and some linear combination of the columns of $\mathbf{M}^{\shortparallel}_{\mathrm{TR}}$:

$$\vec{d} = d_{\nparallel}\vec{v}^{\nparallel}_{\mathrm{TR}} + \mathbf{M}^{\shortparallel}_{\mathrm{TR}}\vec{d}_{\shortparallel}, \tag{39}$$

where the $d_{\text{⊮}}$ and $\vec{d}_{\text{⫫}}$ variables are scaling coefficients. The scaling coefficients $d_{\text{⊮}}$ and $\vec{d}_{\text{⫫}}$ are obtained by projecting the *a priori* measured distances, $\vec{d}_{\text{m}}$, onto $\vec{v}^{\text{⊮}}_{\text{TR}}$ and $\mathbf{M}^{\text{⫫}}_{\text{TR}}$:

$$\begin{bmatrix} d_{\text{⊮}} \\ \vec{d}_{\text{⫫}} \end{bmatrix} = \begin{bmatrix} \vec{v}^{\text{⊮}}_{\text{TR}} & \mathbf{M}^{\text{⫫}}_{\text{TR}} \end{bmatrix}^{\text{T}} \vec{d}_{\text{m}}. \tag{40}$$

For completeness, it should be noted that a similar derivation can be performed to find an equivalent $\vec{v}^{\text{⊮}}_{\text{TR}}$ for the logarithm of the scaled distance vector, $\vec{d}^{\gamma}$. The exclusive use of phase-response data over log-magnitude data was chosen for convenience. Alternatively, both the magnitude and phase information could be used to make a combined estimate. However, the $\vec{d}$ and $\vec{d}^{\gamma}$ vectors are related by a logarithmic function, so combining $\vec{v}^{\text{⊮}}_{\text{TR}}$ estimates requires a nonlinear search. Since satisfactory results are obtained with only phase information, the additional complexity associated with combining distance vector estimates from both magnitude and phase information is omitted in the interest of simplicity.

### *2.4. Linear Solution and Model Null-Space*

The general solution to (12) can be obtained by applying the Moore-Penrose pseudoinverse [18], denoted by "†", and accounting for the null-space of the $\mathbf{A}$ matrix:

$$\mathbf{X} = \mathbf{A}^{\dagger}\mathbf{S}_{\text{m}} + \mathbf{A}^{\neq}\mathbf{C}^{\neq}_{\text{A}}, \tag{41}$$

where $\mathbf{A}^{\dagger} = \left(\mathbf{A}^{\text{T}}\mathbf{A}\right)^{-1}\mathbf{A}^{\text{T}}$, the columns of $\mathbf{A}^{\neq}$ form a basis for the null space of $\mathbf{A}$ and $\mathbf{C}^{\neq}_{\text{A}}$ is a matrix of unknown coefficients. In section 2.2 it was shown that the phase noise has zero mean and the log-magnitude noise can be safely treated as zero mean. As such, the pseudoinverse operation used in (41) provides the least-squares approximation to the values in $\mathbf{X}$. Note that obtaining the first term of (41) is not computationally demanding since the $\mathbf{A}^{\dagger}$ matrix is not frequency-dependent and need only be calculated once.

For the problem formulation considered here, the null space of $\mathbf{A}$ can be characterized by inspection of (13$a$). To begin, decompose the $\mathbf{M}^{\neq}_{\text{TR}}$ matrix into two sub-matrices:

$$\mathbf{M}^{\neq}_{\text{TR}} = \begin{bmatrix} \mathbf{M}^{\neq}_{\text{(T)R}} \\ \mathbf{M}^{\neq}_{\text{T(R)}} \end{bmatrix}, \tag{42}$$

where $\mathbf{M}^{\neq}_{\text{(T)R}}$ is a $[t \times m^{\neq}_{\text{TR}}]$ sub-matrix and $\mathbf{M}^{\neq}_{\text{T(R)}}$ is a $[r \times m^{\neq}_{\text{TR}}]$ sub-matrix. Assuming that $\vec{d}$ and $\vec{d}^{\gamma}$ are linearly independent of $\mathbf{M}_{\text{T}}$ and $\mathbf{M}_{\text{R}}$, then the null space of $\mathbf{A}$ is

spanned by five sets of vectors, namely:

$$\mathbf{A}^{\neq} = \begin{array}{c} \\ (\underline{1}) \\ (\underline{2}) \\ (\underline{3}) \\ (\underline{4}) \\ (\underline{5}) \\ (\underline{6}) \\ (\underline{7}) \\ (\underline{8}) \\ (\underline{9}) \\ (\underline{10}) \end{array} \begin{array}{c} \begin{array}{ccccc} \mathbf{A}_{\mathfrak{R}}^{\neq} & \mathbf{A}_{\mathfrak{I}}^{\neq} & \mathbf{A}_{\tau}^{\neq} & \mathbf{A}_{\rho}^{\neq} & \vec{a}_{\kappa}^{\neq} \end{array} \\ \begin{bmatrix} \mathbf{M}_{(\mathrm{T})\mathrm{R}}^{\neq} & \mathbf{0} & \mathbf{0} & \mathbf{0} & \vec{0}_t \\ \mathbf{0} & \mathbf{M}_{(\mathrm{T})\mathrm{R}}^{\neq} & \mathbf{0} & \mathbf{0} & \vec{0}_t \\ \mathbf{0} & \mathbf{0} & \mathbf{I}_t & \mathbf{0} & \vec{0}_t \\ \mathbf{M}_{\mathrm{T}(\mathrm{R})}^{\neq} & \mathbf{0} & \mathbf{0} & \mathbf{0} & \vec{0}_r \\ \mathbf{0} & \mathbf{M}_{\mathrm{T}(\mathrm{R})}^{\neq} & \mathbf{0} & \mathbf{0} & \vec{0}_r \\ \mathbf{0} & \mathbf{0} & \mathbf{0} & \mathbf{I}_r & \vec{0}_r \\ 0 & 0 & 0 & 0 & 0 \\ 0 & 0 & 0 & 0 & 0 \\ 0 & 0 & 0 & 0 & 1 \\ \mathbf{0} & \mathbf{0} & -\frac{1}{2\pi}\mathbf{M}_{\tau} & -\frac{1}{2\pi}\mathbf{M}_{\rho} & \frac{1}{2\pi}\vec{d} \end{bmatrix} \end{array}. \tag{43}$$

The fact that the columns of $\mathbf{A}^{\neq}$ reside in the null space of $\mathbf{A}$ can be verified by inspection of (13$a$) and (43). To verify that the entire null space of $\mathbf{A}$ is spanned by the columns of $\mathbf{A}^{\neq}$, first note that each column of $\mathbf{A}^{\neq}$ is independent of all other columns, and then consider that there are $2m_{\mathrm{TR}}^{\neq} + t + r + 1$ columns. Since the dimensions of $\mathbf{A}$ are $[3s \times (3(t + r + 1) + s)]$, the rank-nullity theorem states that:

$$\mathrm{rank}\,(\mathbf{A}) + \mathrm{nullity}\,(\mathbf{A}) = 3(t + r + 1) + s, \tag{44}$$

Substituting (16) and (15) into the above equation and solving for $\mathrm{nullity}\,(\mathbf{A})$ yields:

$$\mathrm{nullity}\,(\mathbf{A}) = 2m_{\mathrm{TR}}^{\neq} + t + r + 1. \tag{45}$$

Since there are $2m_{\mathrm{TR}}^{\neq} + t + r + 1$ columns in $\mathbf{A}^{\neq}$ that are linearly independent and reside in the null space of $\mathbf{A}$, these columns span the null space of $\mathbf{A}$.

The first two sets of vectors, $\mathbf{A}_{\mathfrak{R}}^{\neq}$ and $\mathbf{A}_{\mathfrak{I}}^{\neq}$, account for potential ambiguities in the magnitude and phase relationship between the transmitter and receiver transfer functions. Consider a simple example: regardless of the actual phase estimates of the transmitter and receiver transfer functions, no net change would result in the phase estimate of model-generated signals if *all* of the transmitter phase estimates are shifted by some angular offset, $\theta$, and *all* of the receiver phase estimates are shifted by a corresponding negative phase offset, $-\theta$. This type of ambiguity, and the analogous scenario with log-magnitude scaling, is captured by the $\mathbf{A}_{\mathfrak{R}}^{\neq}$ and $\mathbf{A}_{\mathfrak{I}}^{\neq}$ null-spaces. Unless additional constraints are available for $\mathbf{T}_{\mathfrak{I}}$ or $\mathbf{R}_{\mathfrak{I}}$, the sub-space defined by $\mathbf{A}_{\mathfrak{R}}^{\neq}$ and $\mathbf{A}_{\mathfrak{I}}^{\neq}$ can be ignored from an estimation standpoint since the ambiguity cannot be resolved.

The third and fourth sets of vectors, $\mathbf{A}_{\tau}^{\neq}$ and $\mathbf{A}_{\rho}^{\neq}$, relate additional phase offsets in the transmitter and receiver phase estimates with corresponding shifts in the $\vec{b}$ vector estimate. Notice that as the $\mathbf{A}_{\tau}^{\neq}$ and $\mathbf{A}_{\rho}^{\neq}$ columns are scaled by integer multiples of $2\pi$, the resulting phase offsets for the transmitter and receiver transfer functions are changed by integer multiples of $2\pi$, which results in effectively unchanged transmitter and receiver phase responses. Additionally, if the elements of $\mathbf{M}_{\tau}$ and $\mathbf{M}_{\rho}$ are *integer* values, then $2\pi$ integer multiples of $\mathbf{A}_{\tau}^{\neq}$ and $\mathbf{A}_{\rho}^{\neq}$ result in integer shifts in the $\vec{b}$ vector

estimate. This repetitive behavior indicates that the $\measuredangle T(\omega)$, $\measuredangle R(\omega)$, and $\vec{b}$ estimates are not unique. This conclusion is somewhat intuitive since any $2\pi$ offset in $\measuredangle T(\omega)$ or $\measuredangle R(\omega)$ results in an identical set of signals. Unlike the first two sets of vectors, $\mathbf{A}_{\tau}^{\neq}$ and $\mathbf{A}_{\rho}^{\neq}$ cannot be ignored, since they influence the $\vec{b}$ vector estimate.

Finally, the fifth null-space vector set, $\vec{a}_{\kappa}^{\neq}$, is a single vector. If, like the $\mathbf{M}_{\tau}$ and $\mathbf{M}_{\rho}$ matrices that are assumed to have only "1" and "0" elements, the $\vec{d}$ vector can be multiplied by some value to produce an all-integer vector, then the $\kappa$ estimate is not unique. As a result, a unique $\kappa$ solution is only mathematically possible if the $\vec{d}$ vector contains at least one irrational element. Although a requirement for an irrational distance is impractical, it is relatively easy to select a set of distances such that only one solution can be accepted as a realistic parameter value. A lower bound for the proximity of potential solutions was derived by Hall and Michaels [10]. Like the $\mathbf{A}_{\tau}^{\neq}$ and $\mathbf{A}_{\rho}^{\neq}$ vector sets, the $\vec{a}_{\kappa}^{\neq}$ vector also affects the $\vec{b}$ vector estimate and cannot be ignored.

The $\mathbf{A}_{\tau}^{\neq}$, $\mathbf{A}_{\rho}^{\neq}$, and $\vec{a}_{\kappa}^{\neq}$ vector sets all have an impact on the $\vec{b}$ vector estimate. Two additional model constraints can be applied to assist in the $\vec{b}$ vector estimate. First, the assumed model dictates that $\kappa$, $\vec{\tau}$, $\vec{\rho}$, and $\vec{b}$ are all frequency-independent. Therefore, the coefficients in $\mathbf{C}_{\mathrm{A}}^{\neq}$ of (41) that impact the $\kappa$, $\vec{\tau}$, $\vec{\rho}$, and $\vec{b}$ estimates must also be frequency-independent. Additionally, the $\vec{b}$ vector is constrained to be an all-integer vector. To enforce these final constraints in the model parameter estimates, a nonlinear search is required.

### *2.5. Nonlinear Search*

In Section 2.4, the linear least-squares estimate of $\mathbf{X}$ in (41) was shown to include some linear combination of the column vectors described in (43). Of these five sets of vectors, three sets of vectors ($\mathbf{A}_{\tau}^{\neq}$, $\mathbf{A}_{\rho}^{\neq}$, and $\vec{a}_{\kappa}^{\neq}$) are associated with the $\vec{b}$ estimate, which must be an all-integer vector for the estimated model parameters to agree with the data. A nonlinear search is described here to identify a solution that satisfies the all-integer constraint.

The use of an unwrapped phase response ensures that the all-integer $\vec{b}$ vector is frequency-independent. Therefore, a $\vec{b}$ estimate can be described as a function of frequency-independent null-space coefficients, $\vec{c}$:

$$\begin{aligned}\vec{b}(\vec{c}) &= \mathbf{B}\mathbf{X}(\vec{c})\,\vec{\Sigma} \\ &= \mathbf{B}\left(\mathbf{A}^{\dagger}\mathbf{S}_{\mathrm{m}} + \left[\begin{array}{cccc} \mathbf{A}_{\tau}^{\neq} & \mathbf{A}_{\rho}^{\neq} & \vec{a}_{\kappa}^{\neq} \end{array}\right] \vec{c}\;\vec{1}_{w}^{\mathrm{T}}\right)\vec{\Sigma},\end{aligned} \tag{46}$$

where $\mathbf{B} = \left[\begin{array}{cc} \mathbf{0} & \mathbf{I}_s \end{array}\right]$ is a $[s \times 3(t+r+1)+s]$ matrix that isolates the elements of $\mathbf{X}$ corresponding to the $\vec{b}$ values, $\vec{c}\;\vec{1}_{w}^{\mathrm{T}}$ corresponds to the frequency-independent coefficients in $\mathbf{C}_{\mathrm{A}}^{\neq}$, and $\vec{\Sigma}$ is a $[w \times 1]$ vector that performs a weighted average over frequency.

*2.5.1. Optimal Weights* In this section, the optimal weights, $\vec{\Sigma}^{\bullet}$, for combining the frequency-dependent estimates of $\vec{b}$ are derived.

Let $\hat{b}_{\bar{\bar{\mathrm{A}}}}$ be the collection of $w$ separate estimates of $\vec{b}$ obtained by applying the pseudo-inverse of $\mathbf{A}$ to the measurement matrix $\mathbf{S}_{\mathrm{m}}$. Since $\vec{b}$ is independent of frequency, each of these estimates corresponds to a single, underlying vector, $\vec{b}_{\bar{\bar{\mathrm{A}}}}$, plus additive noise:

$$\begin{aligned}\hat{b}_{\bar{\bar{\mathrm{A}}}} &= \mathbf{B}\mathbf{A}^{\dagger}\mathbf{S}_{\mathrm{m}} \\ &= \mathbf{B}\mathbf{A}^{\dagger}\mathbf{S} + \mathbf{B}\mathbf{A}^{\dagger}\mathbf{N} \\ &= \vec{b}_{\bar{\bar{\mathrm{A}}}}\vec{1}_w^{\mathrm{T}} + \mathbf{N}_{\mathrm{b}}. \end{aligned} \tag{47}$$

where $\mathbf{S}_{\mathrm{m}}$ is defined in (33) and $\mathbf{N}_{\mathrm{b}}$ is another $[s \times w]$ matrix of additive noise constructed as $\mathbf{B}\mathbf{A}^{\dagger}\mathbf{N}$. Since each element of $\mathbf{N}_{\mathrm{b}}$ is constructed from a linear combination of the elements of $\mathbf{N}$, the noise present in each element of $\mathbf{N}_{\mathrm{b}}$ has effectively zero mean. In addition, since each column of $\mathbf{N}$ is independent of the others, each column of $\mathbf{N}_{\mathrm{b}}$ is also independent of the other columns in $\mathbf{N}_{\mathrm{b}}$.

The optimal weights, $\vec{\Sigma}^{\bullet}$, are selected to satisfy:

$$\vec{\Sigma}^{\bullet} = \arg\min_{\vec{\Sigma}} E\left[\left\|\hat{b}_{\bar{\bar{\mathrm{A}}}}\vec{\Sigma} - \vec{b}_{\bar{\bar{\mathrm{A}}}}\right\|^2\right], \qquad \text{such that} \qquad \vec{1}_w^{\mathrm{T}}\vec{\Sigma} = 1, \tag{48}$$

where $E[\cdot]$ is the expected value operator and the $\vec{1}_w^{\mathrm{T}}\vec{\Sigma} = 1$ constraint ensures that the weights sum to 1. The solution to (48) can be found using a Lagrange multiplier, $\lambda$, to satisfy the summation constraint,

$$L = E\left[\left(\hat{b}_{\bar{\bar{\mathrm{A}}}}\vec{\Sigma} - \vec{b}_{\bar{\bar{\mathrm{A}}}}\right)^{\mathrm{T}}\left(\hat{b}_{\bar{\bar{\mathrm{A}}}}\vec{\Sigma} - \vec{b}_{\bar{\bar{\mathrm{A}}}}\right)\right] + \lambda\left(\vec{\Sigma}^{\mathrm{T}}\vec{1}_w - 1\right). \tag{49}$$

The Lagrangian, $L$, is minimized by taking the derivative of (49) with respect to $\vec{\Sigma}$, setting it equal to zero, and solving for $\vec{\Sigma}$:

$$\vec{\Sigma}^{\bullet} = \mathbf{Z}^{-1}\vec{1}_w\left(\left\|\vec{b}_{\bar{\bar{\mathrm{A}}}}\right\|^2 - \frac{\lambda}{2}\right), \tag{50}$$

where

$$\mathbf{Z}^{-1} = \left(\left\|\vec{b}_{\bar{\bar{\mathrm{A}}}}\right\|^2 \vec{1}_w\vec{1}_w^{\mathrm{T}} + \mathbf{\Lambda}_{\mathrm{N}}\right)^{-1} \tag{51}$$

and

$$\begin{aligned}\mathbf{\Lambda}_{\mathrm{N}} &= E\left[\mathbf{N}_{\mathrm{b}}^{\mathrm{T}}\mathbf{N}_{\mathrm{b}}\right] \\ &= \begin{bmatrix} \sigma_{\mathrm{b}1}^2 & 0 & \cdots \\ 0 & \sigma_{\mathrm{b}2}^2 & \\ \vdots & & \ddots \end{bmatrix}. \end{aligned} \tag{52}$$

Note that a large reduction in terms during the Lagrangian minimization is possible because $E[\mathbf{N}_{\mathrm{b}}] = \mathbf{0}$. Each $\sigma_{\mathrm{b}i}^2$ element corresponds to $E\left[\begin{array}{cc} \vec{N}_{\mathrm{b}i}^{\mathrm{T}} & \vec{N}_{\mathrm{b}i} \end{array}\right]$, where $\vec{N}_{\mathrm{b}i}$ is the $i$th column vector of $\mathbf{N}_{\mathrm{b}}$. Substituting (50) into the $\vec{1}_w^{\mathrm{T}}\vec{\Sigma} = 1$ constraint of (48), $\left\|\vec{b}_{\bar{\bar{\mathrm{A}}}}\right\|^2 - \frac{\lambda}{2}$ can be found:

$$\left(\left\|\vec{b}_{\bar{\bar{\mathrm{A}}}}\right\|^2 - \frac{\lambda}{2}\right) = \frac{1}{\vec{1}_w^{\mathrm{T}}\mathbf{Z}^{-1}\vec{1}_w}. \tag{53}$$

Finally, a closed-form solution to (48) is obtained by substituting (53) into (50):

$$\vec{\Sigma}^{\bullet} = \frac{\mathbf{Z}^{-1}\vec{1}_w}{\vec{1}_w^{\mathrm{T}}\mathbf{Z}^{-1}\vec{1}_w} \propto \left[ \begin{array}{ccc} \frac{1}{\sigma_{\mathrm{b}1}^2} & \frac{1}{\sigma_{\mathrm{b}2}^2} & \cdots \end{array} \right]^{\mathrm{T}}. \tag{54}$$

The proportionality with the inverse noise variance can be seen by noting that the structure of $\mathbf{Z}^{-1}$ naturally lends itself to the Woodbury Matrix Identity [19], also known as the matrix inversion lemma. According to this identity formula, $\mathbf{Z}^{-1}$ can be calculated as:

$$\mathbf{Z}^{-1} = \mathbf{\Lambda}_{\mathrm{N}}^{-1} - \frac{\mathbf{\Lambda}_{\mathrm{N}}^{-1}\vec{1}_w\vec{1}_w^{\mathrm{T}}\mathbf{\Lambda}_{\mathrm{N}}^{-1}}{\frac{1}{\left\|\vec{b}_{\mathrm{A}}^{=}\right\|^2} + \vec{1}_w^{\mathrm{T}}\mathbf{\Lambda}_{\mathrm{N}}^{-1}\vec{1}_w} \tag{55}$$

where

$$\mathbf{\Lambda}_{\mathrm{N}}^{-1} = \left[ \begin{array}{ccc} \frac{1}{\sigma_{\mathrm{b}1}^2} & 0 & \cdots \\ 0 & \frac{1}{\sigma_{\mathrm{b}2}^2} & \\ \vdots & & \ddots \end{array} \right]. \tag{56}$$

The relationship expressed in (54) indicates that the optimal weights are proportional to the inverse of the frequency-dependent noise variance. Since $\mathbf{N}_{\mathrm{b}} = \mathbf{B}\mathbf{A}^{\dagger}\mathbf{N}$, the frequency-dependent noise variance can be derived, similar to (35):

$$\begin{aligned} \sigma_{\mathrm{b}i}^2 &= E\left[\vec{N}_{\mathrm{b}i}^{\mathrm{T}}\vec{N}_{\mathrm{b}i}\right] \\ &= E\left[\vec{N}_i^{\mathrm{T}}\mathbf{Y}\vec{N}_i\right] \\ &= \frac{1}{2}\vec{y}^{\mathrm{T}}\left(\frac{1}{\vec{Q}_i}\right), \end{aligned} \tag{57}$$

where $\mathbf{Y} = (\mathbf{A}^{\dagger})^{\mathrm{T}}\mathbf{B}^{\mathrm{T}}\mathbf{B}\mathbf{A}^{\dagger}$, $\vec{y}$ is a $[3s \times 1]$ vector containing the diagonal elements of $\mathbf{Y}$, $\vec{Q}_i$ is a $[3s \times 1]$ vector of squared complex SNR values for the $i$th column of $\mathbf{S}_{\mathrm{m}}$, and the rightmost division operation is an element-wise inversion. The column-specific, squared complex SNR values, $\vec{Q}_i$, can be approximated in a single matrix, $\mathbf{Q}$:

$$\mathbf{Q} \approx \left[ \begin{array}{c} \mathbf{I}_s \\ \mathbf{I}_s \\ \mathbf{I}_s \end{array} \right] \frac{\exp\left(2\mathbf{S}_{\Re}\right) - \vec{\sigma}_{\mathrm{m}}^2\vec{1}_w^{\mathrm{T}}}{\vec{\sigma}_{\mathrm{m}}^2\vec{1}_w^{\mathrm{T}}}, \tag{58}$$

where $\exp\left(2\mathbf{S}_{\Re}\right)$ is an element-wise exponential operation that produces a $[s \times w]$ matrix of squared magnitude values, $\vec{\sigma}_{\mathrm{m}}^2$ is a $[s \times 1]$ vector of complex noise variance measurements corresponding to each received signal, and the division operation is again performed element-wise. The set of three identity matrices accounts for the structure of $\vec{N}_i$ discussed in (34). With $\mathbf{Q}$ obtained as in (58), the optimal weights can be approximated as:

$$\vec{\Sigma}^{\bullet} \propto \left[ \begin{array}{ccc} \frac{1}{\sigma_{\mathrm{b}1}^2} & \frac{1}{\sigma_{\mathrm{b}2}^2} & \cdots \end{array} \right]^{\mathrm{T}} \propto \frac{1}{\vec{y}^{\mathrm{T}}(1/\mathbf{Q})}, \tag{59}$$

with the division operations again performed element-wise. Note that even though each $\vec{b}$ element is specific to one of the received signals, a single, composite $\vec{\Sigma}^{\bullet}$ is used here since data from multiple signals contribute to the $\hat{b}_{\mathrm{A}}^{=}$ estimates of (47).

*2.5.2. Multidimensional Search* The definition of $\vec{b}$ as a function of $\vec{c}$ in (46) can be used to search for a value of $\vec{c}$ that produces an all-integer estimate. The search is performed by finding $\vec{c}_b$ such that:

$$\vec{c}_b = \arg\min_{\vec{c}} \left\| \vec{\varepsilon}(\vec{c}) \right\|^2, \tag{60}$$

where the error function $\vec{\varepsilon}(\vec{c})$ is defined as

$$\vec{\varepsilon}(\vec{c}) = \vec{b}(\vec{c}) - [\![\vec{b}(\vec{c})]\!]. \tag{61}$$

Here $\vec{b}(\vec{c})$ is defined as in (46) and $[\![\cdot]\!]$ is the round function, which rounds each element towards the nearest integer.

Although the nonlinear search can be performed as written, the error surface associated with (61) is multi-dimensional, discontinuous, and has an infinite number of local minima. As such, the *entire* search space of possible $\vec{c}$ values must be evaluated. Such an exhaustive search is computationally demanding and time intensive.

*2.5.3. Modified Search* A modification to the approach described in (60) and (61) was developed to avoid an exhaustive multidimensional search by taking advantage of the null-space structure. Let $\vec{c}_b$ be defined as the true null-space coefficients with the following sub-components corresponding to the $\mathbf{A}_\tau^{\neq}$, $\mathbf{A}_\rho^{\neq}$, and $\vec{a}_\kappa^{\neq}$ matrices from (43):

$$\vec{c}_b = \left[ \begin{array}{ccc} \vec{c}_\tau^{\,\mathrm{T}} & \vec{c}_\rho^{\,\mathrm{T}} & c_\kappa \end{array} \right]^{\mathrm{T}} = \left[ \begin{array}{cc} \vec{c}_{\tau\rho}^{\,\mathrm{T}} & c_\kappa \end{array} \right]^{\mathrm{T}}, \tag{62}$$

where $\vec{c}_{\tau\rho}^{\,\mathrm{T}} = \left[ \begin{array}{cc} \vec{c}_\tau^{\,\mathrm{T}} & \vec{c}_\rho^{\,\mathrm{T}} \end{array} \right]^{\mathrm{T}}$. Then $\vec{b}(\vec{c}_b)$ from (46) can be decomposed as:

$$\begin{aligned} \vec{b}(\vec{c}_b) &= \mathbf{B}\mathbf{A}^{\dagger}\mathbf{S}_{\mathrm{m}}\vec{\Sigma} + \mathbf{B} \left[ \begin{array}{ccc} \mathbf{A}_\tau^{\neq} & \mathbf{A}_\rho^{\neq} & \vec{a}_\kappa^{\neq} \end{array} \right] \vec{c}_b \\ &= \vec{b}_\kappa(c_\kappa) + \vec{b}_{\tau\rho}(\vec{c}_{\tau\rho}), \end{aligned} \tag{63}$$

with the $\vec{b}_\kappa(c_\kappa)$ and $\vec{b}_{\tau\rho}(\vec{c}_{\tau\rho})$ vectors defined as

$$\vec{b}_\kappa(c_\kappa) = \mathbf{B}\mathbf{A}^{\dagger}\mathbf{S}_{\mathrm{m}}\vec{\Sigma} + \frac{c_\kappa}{2\pi}\vec{d}, \tag{64a}$$

$$\vec{b}_{\tau\rho}(\vec{c}_{\tau\rho}) = -\frac{1}{2\pi}\mathbf{M}_{\tau\rho}\vec{c}_{\tau\rho}. \tag{64b}$$

The above equations can be obtained from (63) through the definitions of $\mathbf{A}_\tau^{\neq}$, $\mathbf{A}_\rho^{\neq}$, and $\vec{a}_\kappa^{\neq}$ in (43) and $\mathbf{M}_{\tau\rho}$ from (14*b*). The $\vec{c}_\tau$ and $\vec{c}_\rho$ vectors that make up $\vec{c}_{\tau\rho}$ are associated with the $\mathbf{A}_\tau^{\neq}$ and $\mathbf{A}_\rho^{\neq}$ vector sets, which were shown in Section 2.4 to relate additional phase offsets of the transmitter and receiver transfer functions to corresponding changes in the $\vec{b}$ estimate. Since these phase offsets result in identical solutions as each $\vec{c}_\tau$ and $\vec{c}_\rho$ coefficient is increased by an integer multiple of $2\pi$, a bound can be established on each element of the $\vec{b}_{\tau\rho}(\vec{c}_{\tau\rho})$ vector for certain structures of $\mathbf{M}_{\tau\rho}$. For example, if $\mathbf{M}_{\tau\rho} = \mathbf{M}_{\mathrm{TR}}$, then the $\mathbf{M}_{\tau\rho}$ matrix will have no more than two "1" values per row. Therefore, each element of the $\vec{b}_{\tau\rho}(\vec{c}_{\tau\rho})$ vector can be constrained to lie between $\pm 1$. These boundaries for $\vec{b}_{\tau\rho}(\vec{c}_{\tau\rho})$, combined with (63), provide a bound for each individual element of $\vec{b}(\vec{c}_b)$:

$$[\![\vec{b}_\kappa(c_\kappa)]\!] \le \vec{b}(\vec{c}_b) \le \lceil\!\lceil \vec{b}_\kappa(c_\kappa) \rceil\!\rceil, \tag{65}$$

where $\vec{c}_b$ and $c_\kappa$ are defined as in (62) and the $\lceil\!\lceil \cdot \rceil\!\rceil$ and $\lfloor\!\lfloor \cdot \rfloor\!\rfloor$ operations denote element-wise ceiling and floor operations, respectively. Equation (65) implies that given a scalar value $c_\kappa$, each integer element of $\vec{b}\,(\vec{c}_b)$ must be one of two integer values, either $\lfloor\!\lfloor \vec{b}_\kappa\,(c_\kappa) \rfloor\!\rfloor$ or $\lceil\!\lceil \vec{b}_\kappa\,(c_\kappa) \rceil\!\rceil$, resulting in $2^s$ possible vectors. To determine the appropriate combination of $s$ integer operations, note that (64$b$) requires $\vec{b}_{\tau\rho}\,(\vec{c}_{\,\tau\rho})$ to lie in the column space of $\mathbf{M}_{\tau\rho}$.

Let $c$ represent a potential value of $c_\kappa$. The best combination of integer operations, $\hat{h}$, for a given $c$ is chosen to satisfy:

$$\hat{h}\,(c) = \underset{\vec{h}\in\mathfrak{H}}{\arg\min} \left\| \mathbf{P}^{\text{ᵸ}}_{\tau\rho} \left( f\left( \vec{b}_\kappa\,(c)\,, \vec{h} \right) - \vec{b}_\kappa\,(c) \right) \right\|, \tag{66}$$

where $\vec{h}$ is a binary vector contained in $\mathfrak{H}$, the set of all vectors containing only "1" and "0" elements, and the function $f\left(\vec{b}, \vec{h}\right)$ is performed element-wise:

$$f\,(b_i, h_i) = \begin{cases} \lfloor\!\lfloor b_i \rfloor\!\rfloor & \text{if } h_i = 0, \\ \lceil\!\lceil b_i \rceil\!\rceil & \text{if } h_i = 1. \end{cases} \tag{67}$$

In (66), the $f\left( \vec{b}_\kappa\,(c)\,, \vec{h} \right)$ term is an estimate of the all-integer $\vec{b}\,(\vec{c}_b)$ vector, given a $c_\kappa$ estimate, $c$, and an $\vec{h}$ vector defining the combination of integer operations. The difference operation, $f\left( \vec{b}_\kappa\,(c)\,, \vec{h} \right) - \vec{b}_\kappa\,(c)$, corresponds to the resulting $\vec{b}_{\tau\rho}\,(\vec{c}_{\,\tau\rho})$ estimate from this combination of $c$ and $\vec{h}$. Finally, the projection operation and norm provide a measure of the portion of the $\vec{b}_{\tau\rho}\,(\vec{c}_{\,\tau\rho})$ estimate that cannot be accommodated by the model since $\vec{b}_{\tau\rho}\,(\vec{c}_{\,\tau\rho})$ must reside in the column space of $\mathbf{M}_{\tau\rho}$.

The structure of (66) can be adapted to find the most appropriate $c_\kappa$value:

$$c_\kappa = \underset{c}{\arg\min} \left\| \mathbf{P}^{\text{ᵸ}}_{\tau\rho} \left( f\left( \vec{b}_\kappa\,(c)\,, \hat{h}\,(c) \right) - \vec{b}_\kappa\,(c) \right) \right\|, \tag{68}$$

where $\hat{h}\,(c)$ and $f\left(\vec{b}, \vec{h}\right)$ are defined as in (66) and (67), respectively.

Rearranging (63) and (64$b$), $\vec{c}_{\,\tau\rho}$ is obtained from an estimate of $c_\kappa$:

$$\vec{c}_{\,\tau\rho} = -2\pi \mathbf{M}^{\dagger}_{\tau\rho} \left( f\left( \vec{b}_\kappa\,(c_\kappa)\,, \hat{h}\,(c_\kappa) \right) - \vec{b}_\kappa\,(c_\kappa) \right) + \mathbf{M}^{\neq}_{\tau\rho} \vec{c}_{\,\tau\rho}. \tag{69}$$

Similar to the case for $\mathbf{A}^{\neq}_{\mathfrak{R}}$ and $\mathbf{A}^{\neq}_{\mathfrak{I}}$ discussed in Section 2.4, the $\mathbf{M}^{\neq}_{\tau\rho}$ in the above equation represents a null space that describes the phase offset ambiguity between the transmitter and receiver transfer functions. Without any further model constraints, this null space, like the $\mathbf{A}^{\neq}_{\mathfrak{R}}$ and $\mathbf{A}^{\neq}_{\mathfrak{I}}$ subspaces, can be ignored.

Equation (68) indicates that for every $c$ value considered in the search for $c_\kappa$, an independent $\hat{h}\,(\vec{c})$ must first be found, which requires the comparison of $2^s$ potential $\vec{h}$ vectors. While this one-dimensional search is an improvement over the multidimensional search described in section 2.5.2, it *is* computationally intensive, particularly since $s$ grows exponentially with the number of transducers.

One method to further streamline the nonlinear search is to introduce additional *a priori* information about the *anticipated* values of $\kappa$. For example, nominal values for $\kappa$ can be calculated based on the propagating environment (material, thickness,

propagation mode). Based on these nominal values, the search space for (68) can be limited to values that result in dispersion estimates that are in the vicinity of the nominal values. Note that although *a priori* information is used at this point, it is not being used to estimate parameters, rather the nominal information selects between parameters that satisfy both the measured data and model constraints.

### *2.6. Model-Based Parameter Estimation Summary and Discussion*

The model-based parameter estimation algorithm is summarized in table 2. This table illustrates that although the derivation is somewhat complicated, the implementation is straightforward and tractable. The algorithm is built upon the assumption that the system of linear equations in (12) accurately reflects the behavior of the recorded signals in $\mathbf{S}_{\mathrm{m}}$. The algorithm also assumes that sufficient samples are used to ensure that the phase response can be accurately unwrapped. Note that for the phase response to be accurately unwrapped, the frequencies of interest must span a continuous band of spectral content with positive SNR at each discrete frequency.

In addition to the above assumptions, it may be possible to incorporate additional constraints into the model to further constrain the resulting estimates. For example, realistic dispersion relations for the frequencies of interest may be monotonic and bounds may be available for the first or second derivatives of the transmitter and receiver transfer functions. For the purposes of this paper, however, all parameters are able to be approximated to a satisfactory degree with the imposed constraints and additional constraints are unnecessary complications.

## 3. Experimental Validation

The model-based parameter estimation technique for wave propagation in a homogeneous medium has been applied to two separate experimental data sets: (1) guided waves excited by a single transmitter and recorded by multiple identical receivers at various distances from the transmitter, and (2) guided waves propagating between sensor pairs of a distributed array composed of six PZT transducers, each with independent transmit and receive transfer functions. This section describes the experimental setup, model assumptions, and assumption-specific algorithmic details, and then presents parameter estimation results.

Although the two examples presented here are based on the $S_0$ and $A_0$ guided wave modes, the algorithm is applicable to any wave-based application for which the analyzed signals behave according to the assumed propagation model. From a guided wave perspective, this means that the algorithm is applicable to any frequency-plate thickness product (including Rayleigh or Stonely waves) with higher frequency ranges, wider bandwidths, and higher order modes than presented here *provided that the model assumptions are valid*, which implies that multiple, mode-pure direct arrivals are available that are free of any reflections or extraneous signals.

**Table 2.** Summary of model-based parameter estimation algorithm for characterizing wave propagation in a homogeneous medium.

**Problem Setup**: The application-specific propagation model is determined and all measurements are described in terms of the model parameters.

- Define $\mathbf{M}_{\mathrm{T}}$, $\mathbf{M}_{\mathrm{R}}$, $\mathbf{M}_{\tau}$, and $\mathbf{M}_{\rho}$ based on model assumptions.
- Define $\mathbf{S}_{\mathrm{m}}$, $\vec{\sigma}^{2}_{\mathrm{m}}$ and $\vec{d}_{\mathrm{m}}$ with measured data.
  - Limit frequencies of interest to a continuous spectrum.
  - Positive SNR in each FFT bin.
  - Unwrap phase responses in $\mathbf{S}_{\mathfrak{J}}$.

**Distance Vector Estimation**: *A priori* distance measurements are projected onto data- and model-driven unit-vectors to obtain an estimate of the actual distance vector.

- Compute $\vec{v}^{\,\text{ⱶ}}_{\mathrm{TR}}$ as the eigenvector corresponding to the largest eigenvalue of $\mathbf{P}^{\text{ⱶ}}_{\mathrm{TR}}\mathbf{S}_{\mathfrak{J}}\mathbf{P}_{\Delta}\mathbf{S}^{\mathrm{T}}_{\mathfrak{J}}\mathbf{P}^{\text{ⱶ}}_{\mathrm{TR}}$ as discussed in (37).
- Use (40) to compute coefficients: $\begin{bmatrix} d_{\text{ⱶ}} \\ \vec{d}_{\shortparallel} \end{bmatrix} = \begin{bmatrix} \vec{v}^{\,\text{ⱶ}}_{\mathrm{TR}} & \mathbf{M}^{\shortparallel}_{\mathrm{TR}} \end{bmatrix}^{\mathrm{T}} \vec{d}_{\mathrm{m}}$.
- Estimate distance vector $\vec{d} = d_{\text{ⱶ}}\vec{v}^{\,\text{ⱶ}}_{\mathrm{TR}} + \mathbf{M}^{\shortparallel}_{\mathrm{TR}}\vec{d}_{\shortparallel}$ as in (39).
- Define $\mathbf{A}$ with $\vec{d}$ estimate as shown in (13$a$).

**Nonlinear Search:** The null-space coefficients $\vec{c}_{\,\tau}$, $\vec{c}_{\,\rho}$, and $c_{\kappa}$ are found to augment the linear solution.

- Estimate optimal weighting coefficient $\vec{\Sigma}^{\bullet}$ as in (59).
- Search for $c_{\kappa} = \arg\min_{c} \left\| \mathbf{P}^{\text{ⱶ}}_{\tau\rho} \left( f\left( \vec{b}_{\kappa}(c), \hat{h}(c) \right) - \vec{b}_{\kappa}(c) \right) \right\|$ as in (68), where $\hat{h}(c)$ and $f(\cdot)$ are defined in (66) and (67).
- Compute $\vec{c}_{\,\tau\rho} = -2\pi\mathbf{M}^{\dagger}_{\tau\rho}\left( f\left( \vec{b}_{\kappa}(c_{\kappa}), \hat{h}(c_{\kappa}) \right) - \vec{b}_{\kappa}(c_{\kappa}) \right)$ from (69).

**Final Solution:** Combine nonlinear search results with least-squares solution to obtain final estimate of $\mathbf{X}$.

- Calculate $\mathbf{X} = \mathbf{A}^{\dagger}\mathbf{S}_{\mathrm{m}} + \begin{bmatrix} \mathbf{A}^{\neq}_{\tau} & \mathbf{A}^{\neq}_{\rho} & \vec{a}^{\neq}_{\kappa} \end{bmatrix} \begin{bmatrix} \vec{c}_{\,\tau} \\ \vec{c}_{\,\rho} \\ c_{\kappa} \end{bmatrix} \vec{1}^{\mathrm{T}}_{w}$ as in (41).

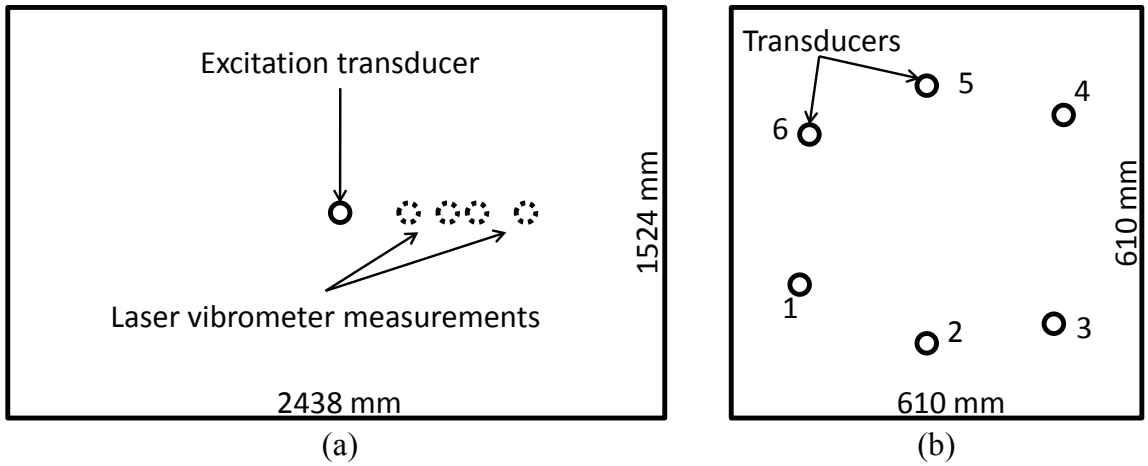


**Figure 3.** Experimental setup for each data set. (a) Guided waves are excited by a single transmitter and recorded at multiple distances with a scanning laser vibrometer. (b) Guided waves are generated with 15 unique transmitter-receiver pairs from a sparse array of six permanently attached transducers.

Algorithmic performance is a challenging concept when working with experimental data since the estimated parameters cannot be compared to "true" parameter values. In previous work [10], the concept of "model fit" was employed, in which the estimated parameters are substituted into the assumed model and the resulting signals are compared with measured data. This technique provides a mechanism to gauge how well the assumed model and estimated parameters are able to describe the measured data. Presumably, if the algorithm is able to accurately describe the measured signals, then the parameters are likely to be accurately estimated. This assumption has been found to be true to a large degree with one exception – in many cases multiple dispersion curve offsets, $\kappa$, can be used to describe the data equally well.

### *3.1. Experimental Setup*

Figure 3 illustrates the experimental setup for the two multi-signal scenarios considered in this paper. For the first set of experimental data, a single PZT transducer excites the two fundamental symmetric, $S_0$, and antisymmetric, $A_0$, modes of a 1524 × 2438 × 3.18 mm plate of 6061 aluminum, which is assumed to be isotropic and homogeneous. Only two modes are excited because the frequency range of the excitation signal is below the cutoff frequency of higher-order modes [20]. The signals are recorded by a scanning laser vibrometer at distances of 545 mm, 606 mm, 626 mm, and 687 mm from the transmitter along a single radial line; therefore $\vec{d}_{\mathrm{m}} = [\ 545 \quad 606 \quad 626 \quad 687\ ]^{\mathrm{T}}$. The measurement distances and plate size were specifically chosen to allow the direct arrival of each mode to be isolated in the time domain without overlap with the other mode or reflections from either mode, which allows each mode to be handled independently by the approach proposed here. Since 200 waveforms were averaged to produce each

measurement, the noise-floor for each laser vibrometer recording was more than 60 dB below the power of the largest frequency component. As such, the $\vec{\sigma}_{\mathrm{m}}^2$ vector elements, for both modes, were set to 0.001 times the power of the largest frequency component in each respective signal.

The second set of experimental data was originally obtained to illustrate sparse array imaging for structural health monitoring by Michaels [21]. A 610 × 610 × 4.76 mm plate of 6061 aluminum, again assumed to be both isotropic and homogeneous, was interrogated with six permanently attached PZT transducers distributed over the surface of the plate, as shown in figure 3(b). If the six transducers are numbered 1-6, then the data collection was performed in the following round-robin fashion: $1 \rightarrow 2$, $1 \rightarrow 3$, $\cdots$, $5 \rightarrow 6$, where $1 \rightarrow 2$ indicates Transducer 1 was used to transmit and Transducer 2 to record the signal, resulting in 15 unique recorded signals. The measured distance vector for the second experimental data set, sorted for readability and expressed in mm, was obtained by measuring the physical distance from transducer to transducer for each transmitter-receiver pair:

$$\begin{aligned}\vec{d}_{\mathrm{m}} = \; & [156 \quad 170 \quad 183 \quad 197 \quad 229 \quad 305 \quad 325 \quad \ldots \\ & 337 \quad 344 \quad 352 \quad 370 \quad 382 \quad 398 \quad 419 \quad 433]^{\mathrm{T}}.\end{aligned} \tag{70}$$

For this second data set, the signals were oversampled and thus occupy a very narrow range in the frequency domain. Therefore, the electronic noise levels, $\vec{\sigma}_{\mathrm{m}}^2$, were estimated by computing the power spectrum of each signal and then selecting the median value. The resulting $\vec{\sigma}_{\mathrm{m}}^2$ vector is:

$$\begin{aligned}\vec{\sigma}_{\mathrm{m}}^2 = \; & [0.047 \quad 0.040 \quad 0.037 \quad 0.060 \quad 0.052 \quad 0.073 \quad 0.038 \quad \ldots \\ & 0.040 \quad 0.098 \quad 0.088 \quad 0.046 \quad 0.034 \quad 0.068 \quad 0.031 \quad 0.098]^{\mathrm{T}},\end{aligned} \tag{71}$$

where each element of $\vec{\sigma}_{\mathrm{m}}^2$ above corresponds to the propagation distance in (70). Note that the noise floor varies slightly between transducer pairs and is not dependent on propagation distance. Although the transducers do excite both $S_0$ and $A_0$ modes, the $S_0$ mode is sufficiently dominant to treat the recorded signals as single-mode. All boundary reflections were removed from the recorded waveforms by windowing the direct arrivals.

Signal processing was performed with MATLAB (The Mathworks, Natick, MA) running on a Hewlett-Packard laptop (Hewlett-Packard Co., Palo Alto, CA) with an Intel Core2 Duo CPU (Intel Corp., Santa Clara, CA) operating at 2.26 GHz with 4 GB of RAM and running Windows Vista Home Premium (Microsoft Corp., Redmond, WA). The model-based parameter estimation algorithm was configured to evaluate 1000 potential $c_\kappa$ values for each algorithm execution, which required less than 1 second to complete for the first data set (four received signals). In contrast, the second data set (15 received signals) required approximately 80 seconds to complete. For both cases, the modified non-linear search described in Section 2.5.3 consumed over 90% of the computation time.

*3.2. Common Transfer Functions*

The first set of model assumptions to be discussed corresponds to the case where the transmit and receive transfer functions are assumed to be identical for all recorded signals, i.e., all signals share a common transmitter and receiver transfer function. Note that because all transmitter and receiver transfer functions are identical, the transmitter and receiver transfer functions cannot be distinguished from one another. As such, the $\mathbf{M}_{\mathrm{R}}$ and $\mathbf{M}_{\rho}$ matrices are null and $\mathbf{M}_{\mathrm{T}} = \mathbf{M}_{\tau} = \mathbf{M}_{\mathrm{TR}} = \mathbf{M}_{\tau\rho} = \vec{1}_s$. Under these assumptions, the structures for $\mathbf{A}$ and $\mathbf{X}$ are:

$$\mathbf{A} = \begin{bmatrix} \vec{1}_s & \vec{0}_s & \vec{0}_s & -\vec{d}^{\,\curlyvee} & \vec{0}_s & \vec{0}_s & \mathbf{0} \\ \vec{0}_s & \vec{1}_s & \vec{1}_s & \vec{0}_s & -\vec{d} & -\vec{d} & 2\pi\mathbf{I}_s \\ \vec{0}_s & \vec{1}_s & \vec{0}_s & \vec{0}_s & -\vec{d} & \vec{0}_s & \mathbf{0} \end{bmatrix}, \qquad \mathbf{X} = \begin{bmatrix} \mathbf{T}_{\mathfrak{R}} + \mathbf{R}_{\mathfrak{R}} \\ \mathbf{T}_{\Delta} + \mathbf{R}_{\Delta} \\ (\vec{\tau} + \vec{\rho})\,\vec{1}_w^{\mathrm{T}} \\ \vec{p}^{\,\mathrm{T}} \\ \vec{k}^{\,\mathrm{T}} \\ \kappa\vec{1}_w^{\mathrm{T}} \\ \vec{b}\vec{1}_w^{\mathrm{T}} \end{bmatrix}. \tag{72}$$

Since the $\mathbf{M}_{\mathrm{TR}}^{\shortparallel}$ matrix is a single vector with identical-valued elements, the final estimate of $\vec{d}$ is obtained by projecting $\vec{d}_{\mathrm{m}}$ onto two unit vectors, $\vec{v}_{\mathrm{TR}}^{\,\curlywedge}$ and $\mathbf{M}_{\mathrm{TR}}^{\shortparallel}$. Note that for the first set of experimental data, two modes are present. Since the propagation distances are identical for both modes, the $\mathbf{S}_{\mathfrak{I}}$ matrix used in (38) is composed of an SNR-weighted sum of the $\mathbf{S}_{\mathfrak{I}}$ for each mode, which ensures that all available data are used to estimate $\vec{d}$.

Analysis of $\mathbf{A}^{\neq}$ reveals that the entire null space of $\mathbf{A}$ is spanned by two vectors, $\mathbf{A}_{\tau}^{\neq}$ and $\vec{a}_{\kappa}^{\neq}$. Since $\mathbf{M}_{\mathrm{TR}} = \vec{1}_s$, the $\mathbf{M}_{\mathrm{TR}}^{\neq}$, $\mathbf{A}_{\mathfrak{R}}^{\neq}$ and $\mathbf{A}_{\mathfrak{I}}^{\neq}$ matrices are null. Similarly, since $\mathbf{M}_{\tau} = \vec{1}_s$ and $\mathbf{M}_{\rho}$ is null, $\mathbf{A}_{\tau}^{\neq}$ is a single vector and $\mathbf{A}_{\rho}^{\neq}$ is null.

Figure 4 reflects the ability of this model to fit the first set of experimental data. The $x$-axis of the waterfall plot corresponds to time, while the $y$-axis reflects propagation distance. Each of the four measured time-domain signals are independently scaled for presentation purposes and are displayed in figure 4 with a vertical offset equal to the measured propagation distance. The estimated signals are generated by substituting the estimated parameters into the propagation model and are presented in a similar fashion, with signal scaling identical to the scaling used for the corresponding measured signals and vertical offset equal to the estimated distances. Errors in distance estimates are manifested as vertical separations between the measured and estimated signals, errors in propagation loss estimates result in amplitude discrepancies, and errors in dispersion or transfer function estimates impact the signal shapes. Figure 4 indicates excellent "model fit" between the estimated model parameters and measured data. Since the same PZT transducer and laser vibrometer were used for all recorded signals, the assumption about identical transmitter and receiver transfer functions is valid. Even if the PZT transducer is not isotropic, the fact that the signals were recorded along a single radial line from the transmitter ensures that the transmitter transfer function is identical for all of the signals.

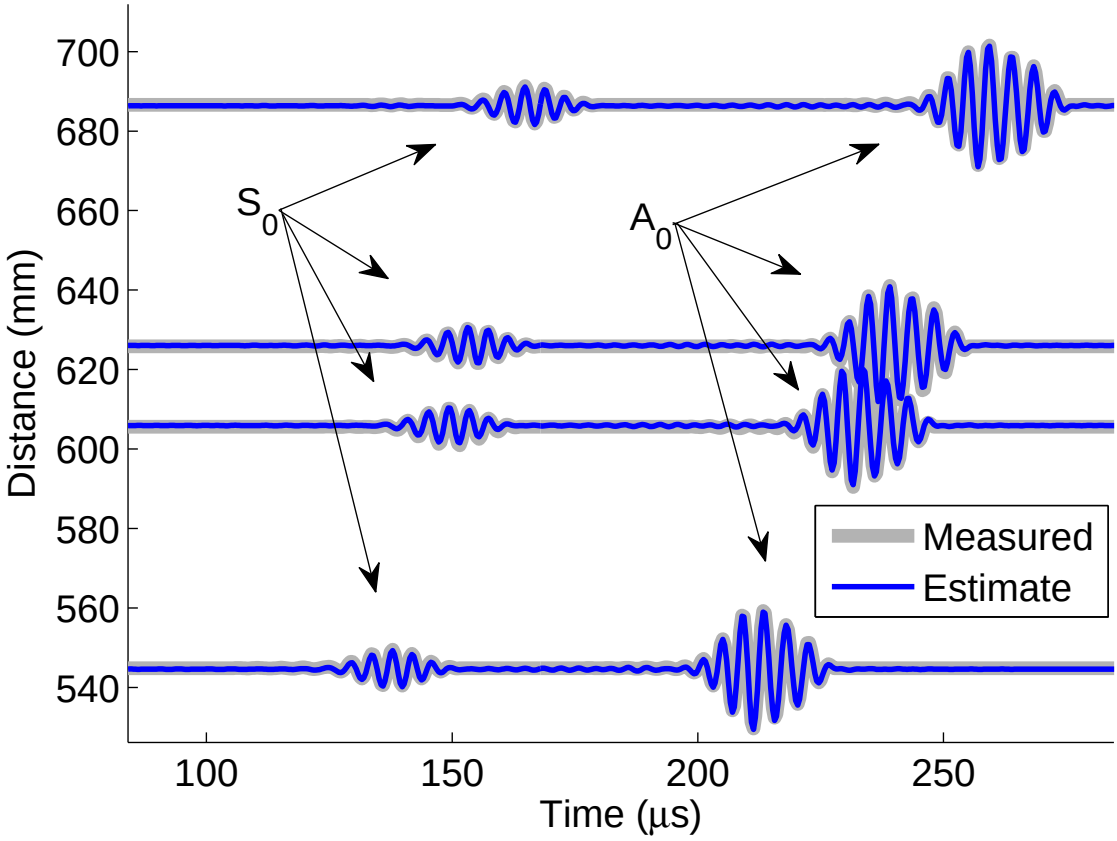


**Figure 4.** Model fit results for experimental data under assumptions that all transmitter and receiver transfer functions are identical. Guided waves are excited by a single transmitter and recorded at multiple distances with a scanning laser vibrometer.

Figure 5 compares the estimated dispersion curves for each mode to nominal dispersion curves for a 3 mm thick aluminum plate. Although a perfect match is not expected because of temperature, pressure, and thickness discrepancies, the estimates closely match the nominal values. Note that with only four received signals, the error surface associated with (68) has an infinite number of periodic local minima. The appropriate $c_\kappa$ was selected by bounding the nonlinear searches to produce a $S_0$ wavenumber between 0 and 0.064 mm$^{-1}$ and an $A_0$ wavenumber between 0.06 and 0.13 mm$^{-1}$ for the lowest frequency considered (156 kHz).

In contrast, figure 6 represents the "model fit" for a model that assumes common transfer functions in each recorded signal when applied to the second set of experimental data, which uses 15 different pairs of six separate transducers. Note that since the number of recorded signals is different for the two data sets, (72) was updated accordingly, which is the only change between the handling of the two data sets. Although all of the transducers are of the same size and shape and similarly bonded to the plate, algorithmic performance is clearly degraded in comparison to figure 4. Significant discrepancies in distance estimates can be seen at the bottom of the figure

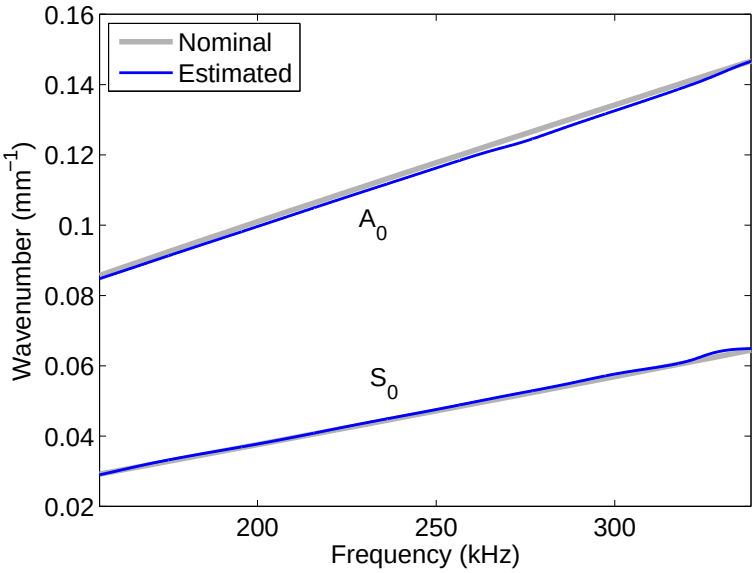


**Figure 5.** Comparison of wavenumber vs. frequency dispersion estimates for experimental data under assumptions that all transmitter and receiver transfer functions are identical. Guided waves are excited by a single transmitter and recorded at multiple distances with a scanning laser vibrometer.

and at roughly 350 mm, where the estimated signals appear offset from the measured signals. Additionally, the signal estimates located at distances less than 200 mm exhibit noticable phase offsets from the measured signals.

### *3.3. Independent Transfer Functions*

In contrast to Section 3.2, the assumed propagation model is expanded to accommodate transducer-specific transmit and receive transfer functions. For the second data set, Transducer 1 is never used to record and Transducer 6 is never used to transmit. Therefore, matrices are defined so that the algorithm estimates five transmitter transfer functions (1-5) and five receiver transfer functions, (2-6), and their respective phase offsets. The $\mathbf{M}_{\mathrm{T}}$, $\mathbf{M}_{\mathrm{R}}$, $\mathbf{M}_{\tau}$, and $\mathbf{M}_{\rho}$ matrices are defined as follows:

$$\mathbf{M}_{\mathrm{T}} = \mathbf{M}_{\tau} = \begin{bmatrix} 1 & 1 & 1 & 1 & 1 & 0 & 0 & 0 & 0 & 0 & 0 & 0 & 0 & 0 & 0 \\ 0 & 0 & 0 & 0 & 0 & 1 & 1 & 1 & 1 & 0 & 0 & 0 & 0 & 0 & 0 \\ 0 & 0 & 0 & 0 & 0 & 0 & 0 & 0 & 0 & 1 & 1 & 1 & 0 & 0 & 0 \\ 0 & 0 & 0 & 0 & 0 & 0 & 0 & 0 & 0 & 0 & 0 & 0 & 1 & 1 & 0 \\ 0 & 0 & 0 & 0 & 0 & 0 & 0 & 0 & 0 & 0 & 0 & 0 & 0 & 0 & 1 \end{bmatrix}^{\mathrm{T}} \tag{73a}$$

$$\mathbf{M}_{\mathrm{R}} = \mathbf{M}_{\rho} = \begin{bmatrix} 1 & 0 & 0 & 0 & 0 & 0 & 0 & 0 & 0 & 0 & 0 & 0 & 0 & 0 & 0 \\ 0 & 1 & 0 & 0 & 0 & 1 & 0 & 0 & 0 & 0 & 0 & 0 & 0 & 0 & 0 \\ 0 & 0 & 1 & 0 & 0 & 0 & 1 & 0 & 0 & 1 & 0 & 0 & 0 & 0 & 0 \\ 0 & 0 & 0 & 1 & 0 & 0 & 0 & 1 & 0 & 0 & 1 & 0 & 1 & 0 & 0 \\ 0 & 0 & 0 & 0 & 1 & 0 & 0 & 0 & 1 & 0 & 0 & 1 & 0 & 1 & 1 \end{bmatrix}^{\mathrm{T}} . \tag{73b}$$

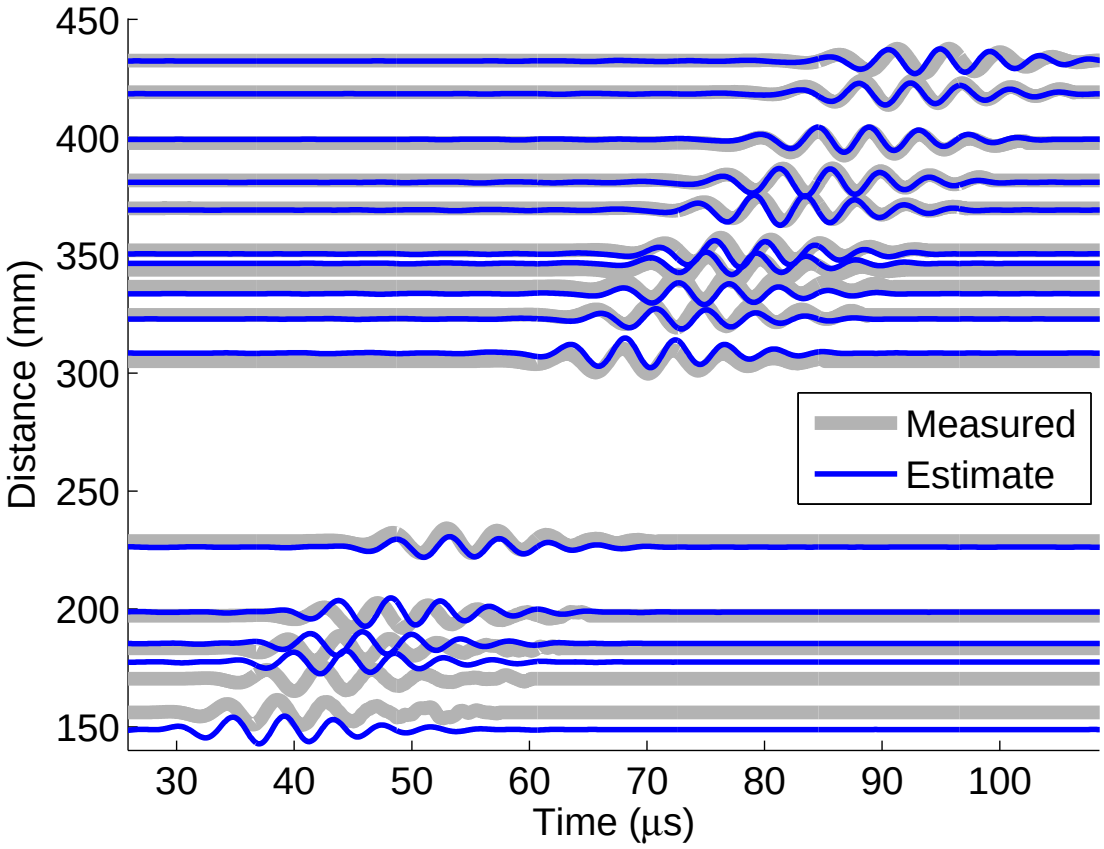


**Figure 6.** Model fit results for experimental data under assumptions that all transmitter and receiver transfer functions are identical. Guided waves were generated with 15 unique transmitter-receiver pairs from a sparse array of six permanently attached transducers.

Unlike the prior case, the $\mathbf{M}_{\mathrm{T}}$ and $\mathbf{M}_{\mathrm{R}}$ matrices defined above have a column-space spanning nine dimensions ($m_{\mathrm{TR}}^{\shortparallel} = 9$), which means that the projection matrix $\mathbf{P}_{\mathrm{TR}}^{\nparallel}$ projects onto a six-dimensional space ($m_{\mathrm{TR}}^{\nparallel} = 15 - m_{\mathrm{TR}}^{\shortparallel} = 6$) and the $\mathbf{M}_{\mathrm{TR}}^{\shortparallel}$ matrix is composed of nine orthonormal vectors. Therefore, the final estimate of $\vec{d}$ is obtained by projecting $\vec{d}_{\mathrm{m}}$ onto a ten-dimensional space (one dimension for $\vec{v}_{\mathrm{TR}}^{\nparallel}$ and nine dimensions for $\mathbf{M}_{\mathrm{TR}}^{\shortparallel}$).

Figure 7 depicts the $\left\|\mathbf{P}_{\tau\rho}^{\nparallel}\left(f\left(\vec{b}_{\kappa}(c), \hat{h}(c)\right) - \vec{b}_{\kappa}(c)\right)\right\|$ values from (68) for both sets of model assumptions. Notice that the more accurate model results in lower error values in general and a stronger indication of the appropriate $c_{\kappa}$.

Figure 8 is analogous to figure 6 for the previous set of model assumptions. However, figure 8 reflects a significantly improved model fit. The additional degrees of freedom in the $\vec{d}$ estimate (ten degrees of freedom vs. two for the common transducer model) allow a much better estimate of the propagation distances. All measured signals appear to be well-approximated, both in shape and amplitude, which indicates accurate estimates of both the independent transfer functions as well as the dispersion curve. The small

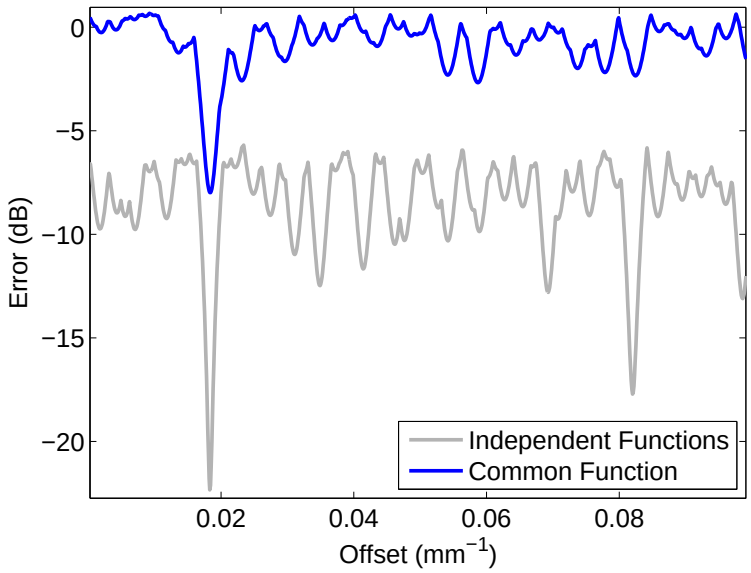


**Figure 7.** Comparison of error metric values for the nonlinear search using experimental data from a sparse array of six transducers. Note that the error is plotted as a function of the $k(\omega)$ estimate for the lowest frequency at which $k(\omega)$ estimation is performed (105 kHz). The overall error is lower and minima are more pronounced for the case of transducer-specific transfer functions.

vertical offsets are attributed to inaccuracies in the distance measurements.

The composite transmitter-receiver transfer functions for each recorded waveform are shown in figure 9. The thick line in the background corresponds to the single estimate of the common transmitter-receiver transfer function from the previous section. The 15 thin lines in the foreground correspond to the 15 independent transmitter-receiver transfer function estimates (i.e. the inverse Fourier transforms of $T_1(\omega) R_2(\omega)$, $T_1(\omega) R_3(\omega)$, $\cdots$, $T_5(\omega) R_6(\omega)$). This figure illustrates that the 15 transducer pairs are best modeled by slightly different transfer functions, which cannot be accommodated by the common transfer function model.

Finally, figure 10 depicts the estimated dispersion curves for the two sets of assumptions. Note that when the model incorporates transducer-specific transfer functions, the dispersion estimate is closer to the expected nominal values. This improvement is not surprising since the model with independent transfer functions represents the received signals more accurately.

## 4. Summary

This paper has presented a model-based approach that estimates wave propagation parameters from a set of recorded signals. A general wave propagation model is presented and a linear system of equations is constructed. Circularly-symmetric complex noise is analyzed in the context of the associated phase and log-magnitude

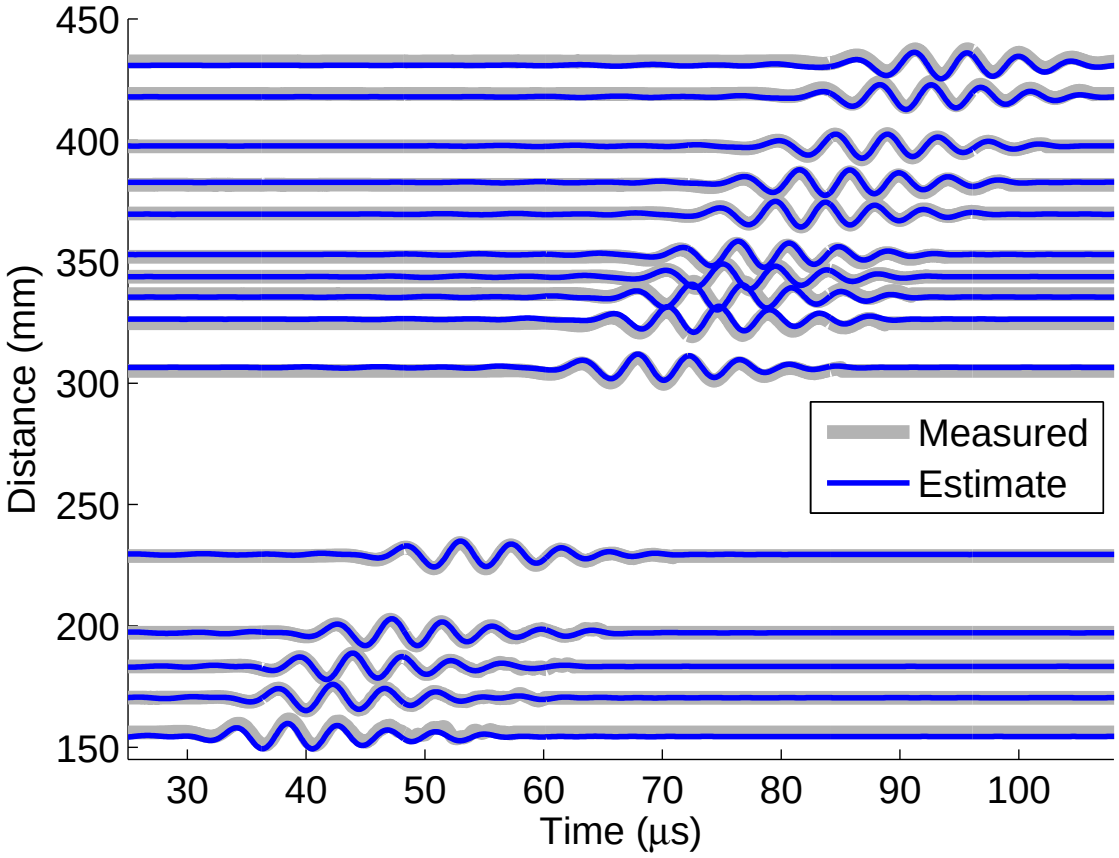


**Figure 8.** Model fit results for experimental data under assumptions that transmitter and receiver transfer functions are transducer-specific. Guided waves were generated with 15 unique transmitter-receiver pairs from a sparse array of six permanently attached transducers.

noise distributions, which are both shown to have effectively zero mean and variances proportional to the square of the complex SNR for SNR values greater than 10 dB. The algorithm obtains a closed-form estimate of the propagation distances by projecting *a priori* measured distances onto two or more orthonormal vectors based on the propagation model and measured data. The remaining model parameters are obtained by first solving a linear system of equations and then augmenting the linear solution with a nonlinear search to incorporate integer-based model constraints. The nonlinear search is performed with a streamlined single-dimensional search. Algorithmic performance is demonstrated with two sets of experimental data using guided waves that correspond to two different sets of model assumptions, demonstrating that the proposed generalized framework can be readily adapted to meet individual application needs.

The primary contribution of this paper is a model-based algorithm for characterizing wave propagation in a homogeneous medium with minimal *a priori* information. This approach allows systems incorporating acoustic, electromagnetic, or elastic waves to characterize dispersion curves, propagation loss, propagation distances, as well as

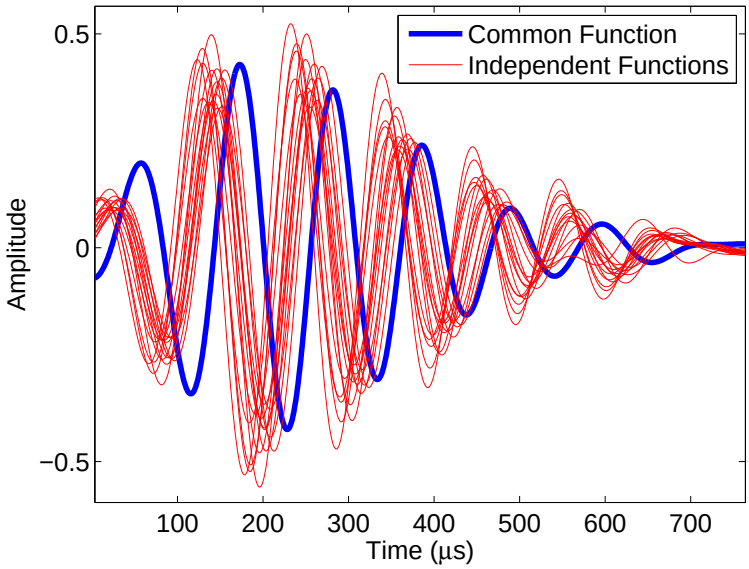


**Figure 9.** Comparison of composite transmitter-receiver transfer functions estimated using experimental data from a sparse array of six transducers. For the common transfer function case, a single transmitted signal is assumed (thick line). When independent transfer functions are modeled, each composite signal is associated with a unique transmitter-receiver combination (thin lines).

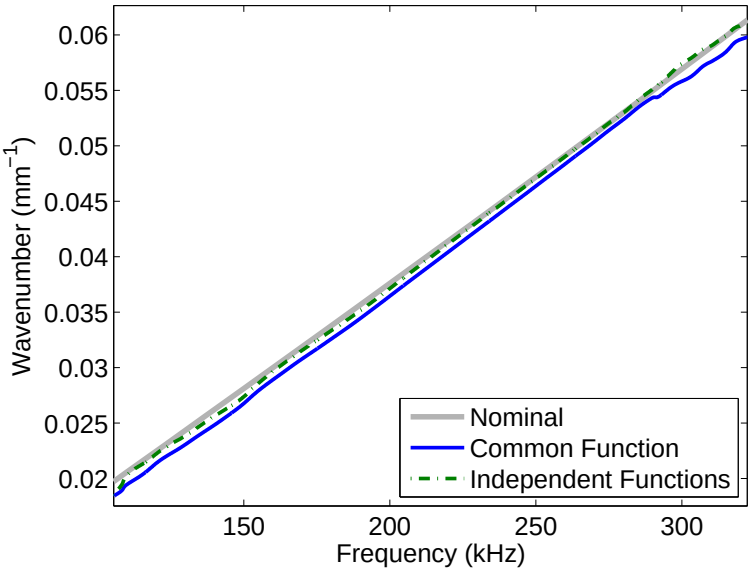


**Figure 10.** Comparison of wavenumber vs. frequency dispersion estimates for experimental data from a sparse array of six transducers. When the model allows for independent transfer functions, the dispersion estimate is closer to nominal values.

transmitter and receiver transfer functions *in situ* at the time of test, thereby avoiding potentially erroneous *a priori* assumptions.

**Acknowledgments**

The authors would like to acknowledge the support of NASA through the Graduate Student Research Program under Grant No. NNX08AY93H, and the Air Force Office of Scientific Research under Grant No. FA9550-08-1-0241.

## References

[1] K. Aki and P. G. Richards. *Quantitative Seismology: Theory and Methods*. W. H. Freeman and Co., San Francisco, 1980.

[2] W. S. Burdic. *Underwater Acoustic System Analysis*. Prentice-Hall, New Jersey, 1984.

[3] C.-P. Chen and W. Sachse. Quantitative acoustic emission source characterization of fatigue cracks in a thin-plate of 7075-T6 aluminum. *J. Appl. Phys.*, 64(11):6264–6273, 1988.

[4] H. N. G. Wadley, C. B. Scruby, and G. Shrimpton. Quantitative acoustic emission source characterisation during low temperature cleavage and intergranular fracture. *Acta Metall. Mater.*, 29(2):399–414, 1981.

[5] T. van Leeuwen and W. A. Mulder. A comparison of seismic velocity inversion methods for layered acoustics. *Inverse Prob.*, 26(1):1–21, 2010.

[6] K. E. Leonard, E. V. Malyarenko, and M. K. Hinders. Ultrasonic Lamb wave tomography. *Inverse Prob.*, 18:1795–1808, 2002.

[7] J. S. Hall and J. E. Michaels. Minimum variance ultrasonic imaging applied to an *in situ* sparse guided wave array. *IEEE Trans. Ultrason., Ferroelectr., Freq. Control*, 57(10):2311–2323, 2010.

[8] S. E. Minkoff and W. W. Symes. Estimating the energy source and reflectivity by seismic inversion. *Inverse Prob.*, 11:383–395, 1995.

[9] T. J. Ulrych. Application of homomorphic deconvolution to seismology. *Geophysics*, 36(4):650–660, 1971.

[10] J. S. Hall and J. E. Michaels. A model-based approach to dispersion and parameter estimation for ultrasonic guided waves. *J. Acoust. Soc. Am.*, 127(2):920–930, 2010.

[11] H. Kwun and K. A. Bartels. Experimental observation of elastic-wave dispersion in bounded solids of various configurations. *J. Acoust. Soc. Am.*, 99(2):962–968, 1996.

[12] W. H. Prosser, M. D. Seale, and B. T. Smith. Time-frequency analysis of Lamb modes. *J. Acoust. Soc. Am.*, 105(5):2669–2676, 1999.

[13] M. Niethammer, L. J. Jacobs, J. Qu, and J. Jarzynski. Time-frequency representation of Lamb waves. *J. Acoust. Soc. Am.*, 109(5):97–102, 2001.

[14] D. Alleyne and P. Cawley. A two-dimensional Fourier transform method for the measurement of propagating multimode signals. *J. Acoust. Soc. Am.*, 89(3):1159–1168, 1991.

[15] W. Sachse and Y.-H. Pao. On the determination of phase and group velocities of dispersive waves in solids. *J. Appl. Phys.*, 49(8):4320–4327, 1978.

[16] J. D. Achenbach. *Wave Propagation in Elastic Solids*. American Elsevier, New York, 1973.

[17] G. Strang. The fundamental theorem of linear algebra. *Am. Math. Mon.*, 100(9):848–855, 1993.

[18] R. Penrose. A generalized inverse for matrices. *P. Camb. Philol. S.*, 51:406–413, 1955.

[19] M. A. Woodbury. Inverting Modified Matrices. *Memorandum Rept. 42, Statistical Research Group, Princeton University*, 1950.

[20] J. L. Rose. *Waves in Solid Media*. Cambridge University Press, 1999.

[21] J. E. Michaels. Detection, localization and characterization of damage in plates with an *in situ* array of spatially distributed sensors. *Smart Mater. Struct.*, 17(035035), 2008.